LA-UR-16-28571
Approved for public release; distribution is unlimited.

Title:	Characterization and Testing of Improved Hydrogen Getter Materials - FY16 Annual Report
Author(s):	Hubbard, Kevin Mark Sandoval, Cynthia Wathen
Intended for:	Report
Issued:	2016-11-07

Characterization and Testing of Improved Hydrogen Getter Materials
FY16 Annual Report

Kevin M. Hubbard and Cynthia W. Sandoval
LANL/MST-7

October 24, 2016

1: Introduction

Organic-based hydrogen getter materials have been in use for many years. These materials are able to prevent the dangerous buildup of hydrogen gas in sealed containers, and are also used to protect surrounding materials from degradation caused by chemical reactions.

Many current getter systems use an acetylenic organic material such as 1,4-bis[phenylethynyl]benzene (DEB) in combination with a carbon-supported palladium catalyst. The structure of DEB is shown in Figure 1-1a. Upon exposure to hydrogen the carbon triple bonds saturate irreversibly to give the aliphatic structure shown in Figure 1-1b. Thus one mole of DEB (278 grams) is capable of trapping four moles of hydrogen gas (89.6 liters at standard temperature and pressure).

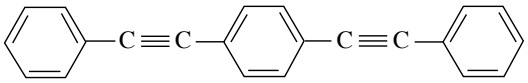

a)

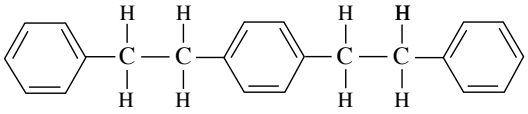

b)

Figure 1-1: Structure of DEB before (a) and after (b) saturation by hydrogen gas.

The organic getter used for DOE applications is typically synthesized by ball-milling a mixture of DEB and carbon-supported palladium, and pressing the mixture into pellet form to attain the desired porosity. The pellets are then loaded into perforated support tubes. The intrinsic performance of the DEB/Pd/C getter has proven adequate, but its use has been limited by the size and geometry of the support tubes. Specifically, the tube configuration prevents the getter from being brought into intimate contact with the materials that either produce hydrogen, or are most sensitive to hydrogen degradation.

There has been a strong desire within DOE to develop an advanced getter system for a variety of future needs. Among other advantages, the new system would be placed in direct contact with emitting sources and/or the materials to be protected, leading to more efficient operation and additional design options.

One successful example is the physical vapor deposition of a DEB/Pd getter composite that uses a Pd organometallic compound as the catalyst. This composite is

prepared under vacuum by the simultaneous sublimation of DEB and sublimation/evaporation of the Pd organometallic [1,2]. The Pd compound used during initial development was allyl-cyclopentadienyl-palladium, or Pd(allyl)Cp, which contains palladium in the Pd(II) valance state. During deposition the substrates were subjected to UV irradiation in order to enhance the catalytic activity of this compound by photolytically reducing the Pd to a metallic state.

The vapor deposition method allows the getter composite to be deposited onto planar or complex surfaces, or infiltrated into porous substrates such as open-celled foams. This provides an opportunity to increase the getter mass and surface area for applications that do not permit the installation of additional getter support tubes. It also allows the getter to be placed in intimate contact with materials that either evolve hydrogen, or are sensitive to hydrogen exposure.

The getter development project has gone through several iterations over the years, and the state of the technology has steadily advanced. Highlights prior to FY16 include:

1) DEB Deposition: The sublimation and recondensation of DEB, without degradation of the reactive triple bonds, was demonstrated. The deposition characteristics were measured as a function of sublimation temperature, system pressure, and carrier gas flow rate. The results were as expected based on theory as long as fresh DEB was added to the sublimation source for every run. Otherwise, grain coarsening progressively decreased the specific surface area of the powder, leading to a steep run-to-run decrease in deposition rate. This effect can be reduced by blending the DEB with SiC grit – the DEB is located interstitially between SiC particles and grain growth is inhibited. Thin films of DEB are found to have a low density, filamentary structure that results in poor infiltration characteristics – a strong thickness gradient is seen in the cross secion of infiltrated porous foams.
2) Pd Deposition: The original Pd precursor had a number of disadvantages, and several alternative compounds were examined as potential replacements. One - (n5-2,4-cyclopentadien-1-yl)[(1,2,3-n)-1-phenyl-2-propenyl]-palladium, or cp-Pd-pp, was selected for further work. Deposition characteristics were measured as a function of sublimation temperature and system pressure. Thin films of cp-Pd-pp are found to be dense and fine grained, and (unlike DEB) the precursor vapor infiltrates efficiently and uniformly into porous foams. As with DEB, the deposition rate is found to decrease with time over the course of a run – in this case due to a compitition between precursor evaporation and decomposition. Evaporation can be favored by running at as low a pressure as possible. The combined results of Tasks 1 and 2 enabled samples with varying DEB/Pd ratios to be systematically prepared and characterized.
3) Characterization of co-deposited DEB-Pd/C: These experiments characterized the performance of getter composite materials infiltrated into open-celled silicone foam under various conditions. Getter loading of up to 2 wt% per run can be obtained. The poor infiltration characteristics of DEB require two runs per sample (reversing the substrate in between) in order to improve compositional uniformity, so that total loading of 4 wt% is possible with the current system. The ability of these samples to getter hydrogen was confirmed by infrared spectroscopy, and hydrogenation of the DEB typically proceeds to 75-85%. Film performance exhibited little/no dependence on DEB/Pd ratio over the range of 9.8-17.0 wt% Pd.

4) Characterization of UV effects: Film performance was characterized as a function of UV exposure during deposition to determine the energy density required for photolytic reduction of pp(Pd)cp. Surprisingly, initial data indicated that the compound is catalytically active even without UV exposure and reduction of the palladium to a metallic state. Furthermore, the use of UV-assisted deposition did not significantly improve getter performance. This discovery has the potential to greatly simplify the processing equipment and methodology.
5) Getter Behavior of Pure cp-Pd-pp: Experiments on the effects of UV exposure also demonstrated that cp-Pd-pp itself acts as a hydrogen getter under the conditions studied. The data indicate that the pristine powder hydrogenates to nearly100% completion, with the formation of volatile cyclopentane as a product. More moles of gas are removed by this reaction than liberated, so pressure buildup will not occur. However, the presence of cyclopentane may be problematic for many applications. Initial data on vapor-deposited cp-Pd-pp films (and films co-deposited with DEB) indicate that the reaction is more limited in this case, perhaps suggesting partial decomposition of the pp(Pd)cp during evaporation/deposition. It is not yet clear if cyclopentane is produced in this case.
6) Alternative deposition methods: A series of experiments was performed in order to study solution deposition of the getter composite as a potentially simpler alternative to vapor deposition. This process involves dissolution of DEB and a Pd organometallic compound in an organic solvent, immersion of a foam part in the solution, and finally removal of solvent from the foam by evaporation. It is possible to achieve getter loading of up to 10 wt% by this method, and the deposited composite reacts to 80-90% completion. These results demonstrate that solution infiltration may be a viable alternative to vapor deposition, potentially eliminating the need for expensive and complex vacuum equipment.

Both vapor- and solution-based processes have been demonstrated to be viable methods for the infiltration of getter composite into open-celled foams. Two examples illustrate the practical performance provided by infiltration of M9763 silicone foams prepared at KCNSC. The vapor deposition process as currently configured can provide a loading of 2 wt%, which is doubled by reversing the foam and performing a second deposition in order to improve uniformity. This would enable a 100 g piece of infiltrated foam to eliminate approximately 33 mmole of hydrogen gas (0.79 liters at STP). Second, solution infiltration can achieve loading of 10 wt%. This would enable the elimination of 95 mmole of hydrogen (2.3 liters at STP) for every 100 g of infiltrated foam.

Work on both infiltration methods continued for FY16:

Solution Infiltration: To date, solution infiltration experiments have primarily made use of toluene as the organic solvent, as it provides good solubility for both DEB and the Pd organometallic. However, toluene does cause considerable swelling of silicone foams, raising concerns of potential degradation of mechanical properties. Most of the FY16 effort was therefore devoted to evaluating potential new solvents that, based upon literature data, might avoid this issue. Solubility was qualitatively evaluated for the DEB/Pd mixture to determine if these solvents produced a true solution, or merely a particle suspension. In either case samples were prepared for characterization that included IR spectroscopy (for molecular structure), electron microscopy (for morphology

and elemental mapping), and quantitative getter performance. Finally, preliminary data were obtained on the mechanical properties of silicone foam before and after extended exposure to pure toluene.

Vapor Infiltration: Prior development of the vapor deposition method has revealed two fundamental (and related) issues that must be resolved.

Effects of UV exposure: It is evident that UV photolysis and reduction of cp-Pd-pp is not necessary in order for the Pd to become catalytically active. The ability to co-deposit an effective getter material without the need for UV exposure would greatly simplify, and reduce the cost of, the deposition process. However, UV exposure may still affect the deposition chemistry and the resulting getter stability/aging behavior. In order to explore this issue in more detail, the relatively low-power mercury vapor lamps originally used were replaced with UV LEDs that enabled much higher power densities. Samples were prepared with and without UV LED exposure and characterized by IR spectroscopy (for molecular structure), ion beam backscattering (for composition), and for quantitative getter performance (both reaction rate and degree of reaction).

Structure and Hydrogenation of Deposited cp-Pd-pp: As mentioned above, the Pd organometallic compound cp-Pd-pp is also capable of reacting with hydrogen gas, both in the as-received state and after vapor deposition. Data for the as-received powder are consistent with nearly complete reaction and the formation of volatile cyclopentane. This is less likely to be true for vapor deposited material, due to partial decomposition during evaporation. However, the presence of cyclopentane (or other organic reaction products) may have a negative effect on material stability, compatibility, and aging. Therefore a number of experiments were performed in an effort to determine the molecular structure and composition of vapor-deposited cp-Pd-pp, the degree to which it acts as a hydrogen getter, and whether or not hydrogenation produces volatile products.

2: Characterization of Getter Performance

The system used to quantify getter performance is shown schematically in Figure 2-1. It operates by measuring the hydrogen pressure and temperature within the sample chamber as a function of time. After sample insertion the system is evacuated to a pressure of 50 mTorr using an oil-free mechanical pump. The valve to the pump is then closed, and the sample chamber is isolated. The remainder of the system is then brought to a pressure of 600 Torr of pure hydrogen, and the valve between the gas regulator and gas reservoir is closed to isolate the system from the hydrogen source. The valve to the sample chamber is then opened, exposing the sample to hydrogen at a known pressure. The pressure and temperature are monitored as a function of time using a National Instruments data logger. Knowing the precise volume of each part of the system, the total number of moles of hydrogen present can be calculated as a function of time using the ideal gas law. Thus the number of moles of gettered hydrogen per mass of sample can be determined.

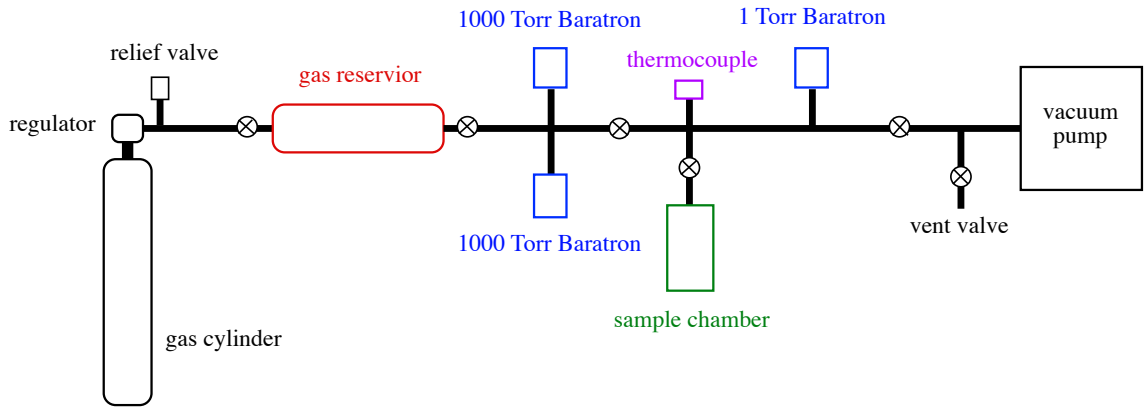

Figure 2-1: Schematic illustration of the system used to quantify getter performance by measuring temperature and hydrogen pressure as a function of time in a sealed system.

The test condition of 600 Torr of pure hydrogen is not representative of typical applications. Several control experiments were therefore performed in order to assure that such a high pressure of hydrogen would not lead to spurious measurements. Specifically, it was necessary to demonstrate that hydrogen would not react with pure DEB or silicone foam at this pressure. Pressure vs. time data for these control materials are shown in Figure 2-2. The data confirm that neither material reacts with hydrogen even at 600 Torr.

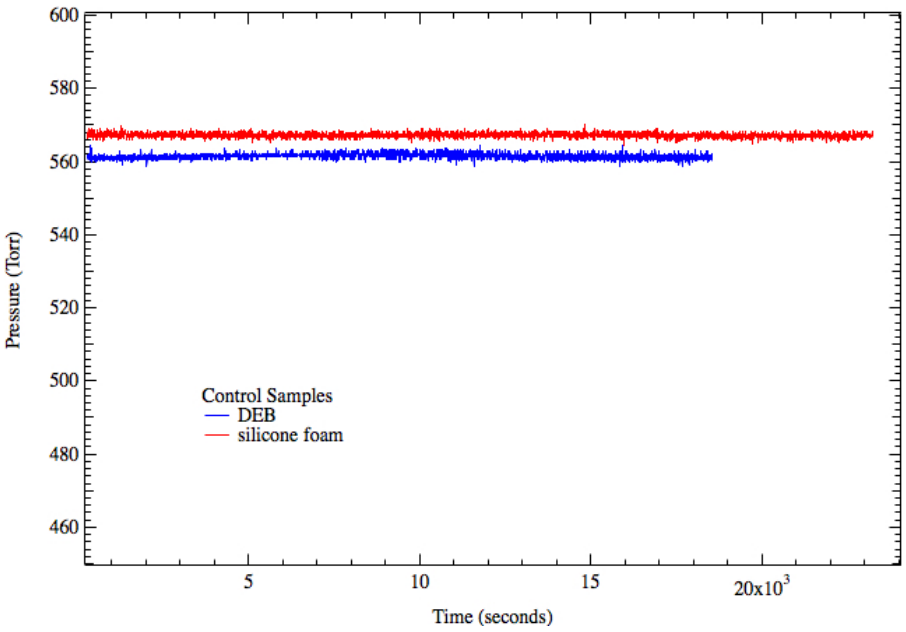

Figure 2-2: Pressure vs. time data taken for two control samples – pure DEB and pristine silicone foam.

Data for a second control test are shown in Figure 2-3 for two samples. The first is silicone foam infiltrated with DEB, and then coated with a 72 nm thick layer of pure Pd by electron-beam evaporation. The second is pristine silicone foam coated with the same thickness Pd layer. The data for the first sample clearly show that the Pd layer effectively catalyzes the formation of atomic hydrogen, which then readily reacts with the DEB. In contrast, no significant pressure change is seen for the second sample. This demonstrates that the pristine silicone foam does not react/degrade even in the presence of atomic hydrogen at 600 Torr.

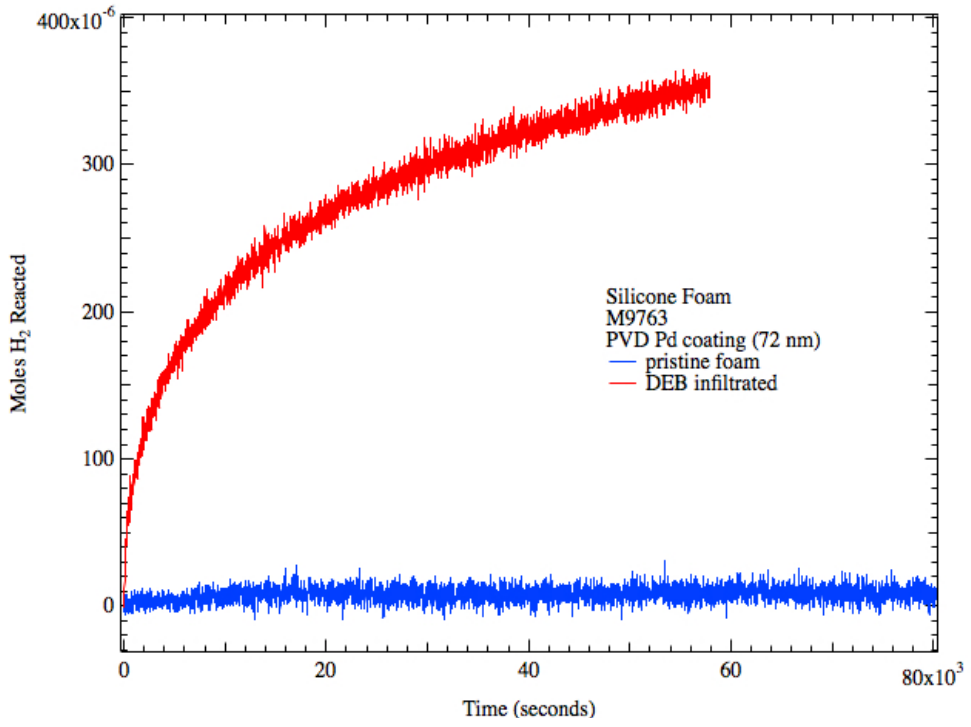

Figure 2-3: Pressure vs. time data for DEB infiltrated silicone foam that was coated with a 72 nm thick Pd film by electron beam evaporation. Data for silicone foam with only the Pd coating are shown for comparison.

The two control tests help assure that pressure changes measured for getter composite samples are caused by dissociation of molecular hydrogen catalyzed by the organometallic Pd catalyst, followed by reaction of the atomic hydrogen with the DEB or with the organic ligands from the Pd organometallic.

3: Solution Deposition Studies

3a: Experimental Procedures

Solution deposition is based on the use of an organic compound that acts as a solvent for both DEB and the Pd organometallic catalyst, but not for the silicone substrate. A solution of the desired concentration and DEB/Pd ratio is prepared and the foam

substrate is immersed for a fixed period of time. The foam is then removed and the solvent allowed to evaporate under (in this case) ambient conditions. The result is ideally an intimately mixed DEB/Pd composite layer uniformly infiltrated throughout the foam substrate.

The Pd catalyst used for most of the experiments is bis(dibenzylideneacetone)Pd, or Pd-dba. The structure of this molecule is shown in Figure 3-1. This compound is of particular interest because the Pd atom is present in a zero (metallic) valance state. Furthermore it is not particularly volatile, so long-term stability of the getter composite should not be an issue.

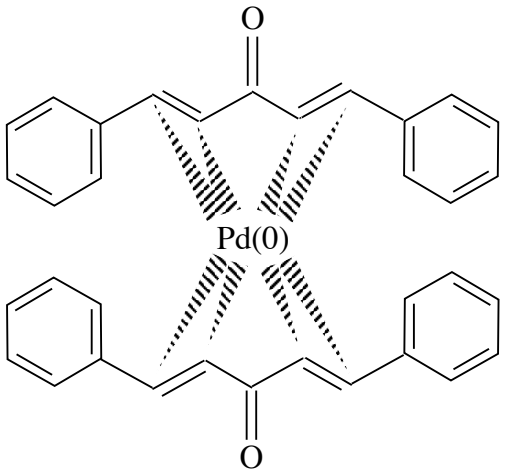

Figure 3-1: Molecular structure of the Pd organometallic precursor bis(dibenzylideneacetone)Pd, or Pd-dba.

The initial proof-of-principle experiments for solution infiltration primarily used toluene as the organic solvent, because it was found to readily dissolve both DEB and Pd-dba. Another intriguing property of toluene is that it is known to swell silicone, with a swelling ratio of 1.3 x [3]. The potential therefore exists to infiltrate the getter/catalyst blend at an almost molecular level, as illustrated schematically in Figure 3.2. This should help securely anchor the composite to the foam matrix for improved adhesion, and also provide intimate mixing of the getter and catalyst. However there is the potential for extended toluene exposure to degrade the silicone foam itself. Previous experiments have shown a mass loss of 1.65% for silicone foam exposed to toluene for a period of 27 hours. The mass loss is most likely from residual unpolymerized resin, or catalyst. However there is the potential for damage to the polymer network and loss of mechanical strength. Furthermore toluene is moderately hazardous. Because it would be necessary to use large quantities in a production environment, it would be desirable to use a solvent with a lower health/environmental impact.

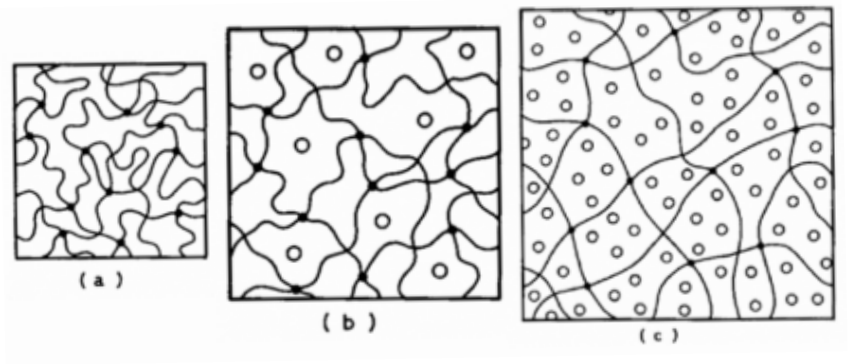

Figure 3-2: Schematic illustration of polymer swelling [4].

Because of the potential disadvantages of using toluene, and also a desire for even higher DEB/Pd solubility, a series of experiments was performed in order to evaluate a number of alternative solvents. The alternatives were chosen on the basis of solubility parameter, silicone swelling behavior, health/environmental impact, or some combination of these three factors. The chosen solvents were:

acetone;
ethanol;
cyclohexane (CH);
hexafluorobenzene (HFB);
FC-84;
perfluorodecalin (PFD);
perfluoro-dimethylcyclohexane (PFMCH).

In each case, solutions were prepared by mixing 400 mg of DEB and 161 mg of Pd-dba with 57 mL of solvent. The DEB/Pd-dba ratio was chosen to provide a nominal 5.32 wt% Pd in the final getter/catalyst composite. The mixtures were blended using an ultrasonic bath for 1-2 hours, followed by magnetic stirring overnight. The solubility of DEB was found to be very poor in FC-84, PFD, and PFMCH. These mixtures produced only very coarse suspensions – milky in appearance with light-colored particulates (DEB) – and were not further considered.

Infiltrated samples were prepared from the rest of the mixtures. The foam substrates were open-cell M9763 silicone prepared at KCNSC, with the following properties:

thickness = 3 mm;
porosity = 63%;
200-400 micron diameter interconnected voids;
surface area = 0.046 m^2/g;
bulk density = 0.4 g/cm^3;
→ a uniform 0.5 micron thick film would provide 5 wt% loading.

Foam coupons of size 1.5 cm x 3.5 cm were weighed and then placed in sealed vials of each of the mixtures, under magnetic stirring, for a period of 27 hours. The coupons were then removed, and the solvent was allowed to evaporate under ambient conditions in a fume hood. In some cases the residual coating included loose particulates on the foam surface.

These particulates were removed from the sample so that the remaining material was robust, with good adhesion. These samples were then reweighed in order to determine the final getter loading.

Characterization of the infiltrated samples included electron microscopy for morphology and elemental mapping, measurement of getter performance by pressure vs. time measurements, and IR spectroscopy for molecular structure before and after hydrogenation. The most useful/interesting samples were prepared from toluene, ethanol, and cyclohexane. Only data from these samples will be presented below.

3b: Results – Reference Materials

There were considerable differences observed in the physical appearances of the solvent / DEB / Pd-dba mixtures:

Toluene – very dark purple/brown, transparent, a true solution;

Ethanol – purple/brown, a milky fine suspension;

Cyclohexane – purple/brown, a milky very fine suspension.

Only toluene was found to be an effective solvent for both DEB and Pd-dba, potentially enabling molecular-level blending of the two compounds. Both ethanol and cyclohexane appear to provide limited dissolution of DEB, forming fine suspensions. This will inherently limit to some extent the degree of getter/catalyst mixing achievable with these solvents. Particle sizes were not measured, although cyclohexane did appear to form a finer suspension.

Analysis was initially performed on four reference powder samples:

- pristine Pd-dba;
- a DEB/Pd-dba blend dry-mixed with a mortar and pestle;
- DEB/Pd-dba recrystallized from toluene;
- DEB/Pd-dba recrystallized from cyclohexane.

The reaction of pristine Pd-dba with hydrogen is shown as a function of time in Figure 3-3. It is found that pure Pd-dba does react with hydrogen under the conditions tested, albeit slowly. After 21 hours the extent of reaction is found to be 1.30 mole H_2/mole Pd-dba. For comparison, reference to the structure shown in Fig. 3-1 shows that reaction of up to 4 mole H_2/mole Pd-dba is theoretically possible (ignoring potential hydrogenation of the aromatic rings). Given sufficient time it is possible that this level of reaction would have been reached.

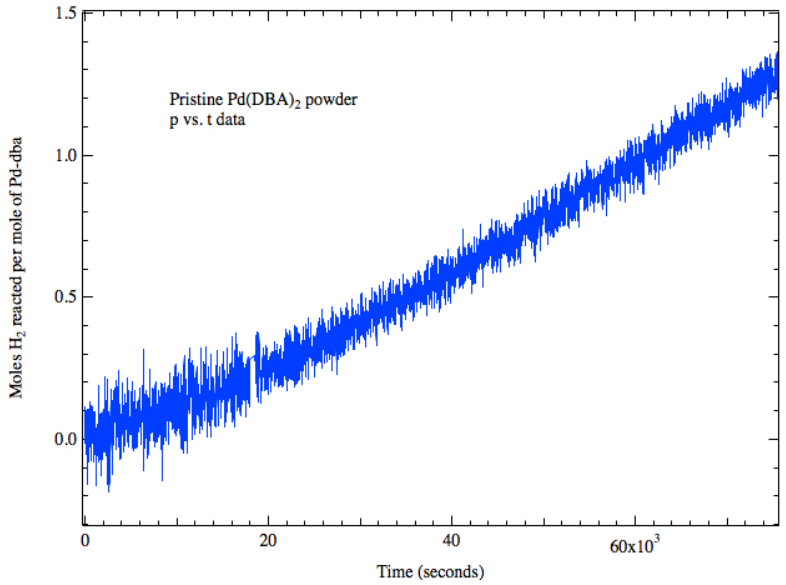

Figure 3-3: Data showing the extent of reaction between hydrogen and pristine Pd-dba as a function of time.

Infrared absorption data for Pd-dba before and after hydrogenation are shown in Figure 3-4. The appearance of absorption bands for single-bonded $-CH_2-$ confirms saturation of the dba double bonds upon exposure to hydrogen. The absorption band at 3025 cm^{-1} is attributed to aromatic CH. The increase in absorption for this feature reflects an increase in absorption strength caused by the change in local charge distribution upon saturation of the adjacent double bond.

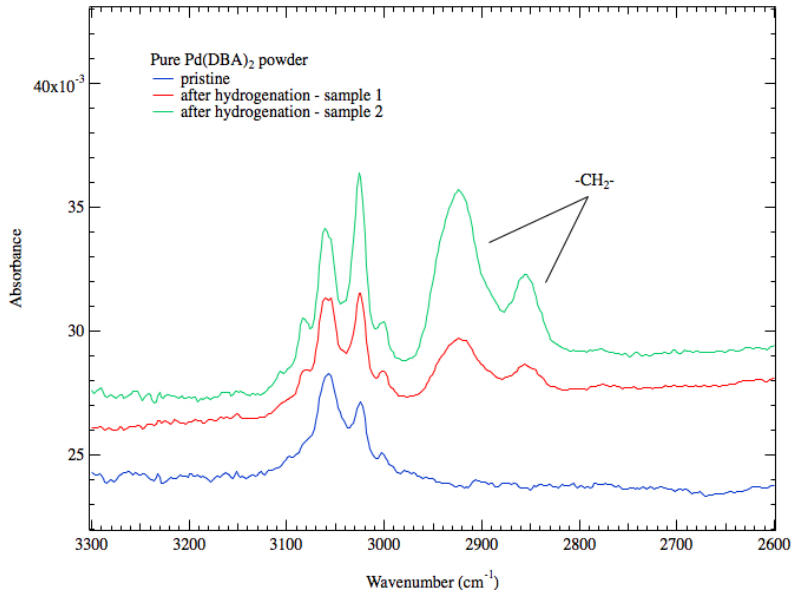

Figure 3-4: IR absorption spectra for Pd-dba, both before and after hydrogenation.

Figure 3-5 shows reaction vs. time data for the other three reference samples, normalized to the nominal DEB content. An interesting range of behavior is observed. For the dry mixed blend there is an "incubation" period of about 30-40 minutes, followed by a moderately fast reaction. This behavior suggests that mixing of the getter and catalyst in this sample is not particularly intimate, certainly not at the molecular level. Nonetheless the calculated extent of reaction for the dry mixed sample is found to be 131% (with respect to DEB content), which suggests considerable hydrogenation of the Pd-dba compound. This is confirmed by the IR absorption spectra shown in Figure 3-6. Spectra are shown for the blend both before and after hydrogenation, with the peaks attributed to Pd-dba highlighted. Comparison of the spectra shows a dramatic change in the absorption features for Pd-dba, confirming considerable hydrogenation. If it is assumed that the DEB in the blend reacts to 95%, it can then be estimated that the Pd-dba must have reacted to the extent of 3.66 mole H_2/mole Pd-dba, or 92%.

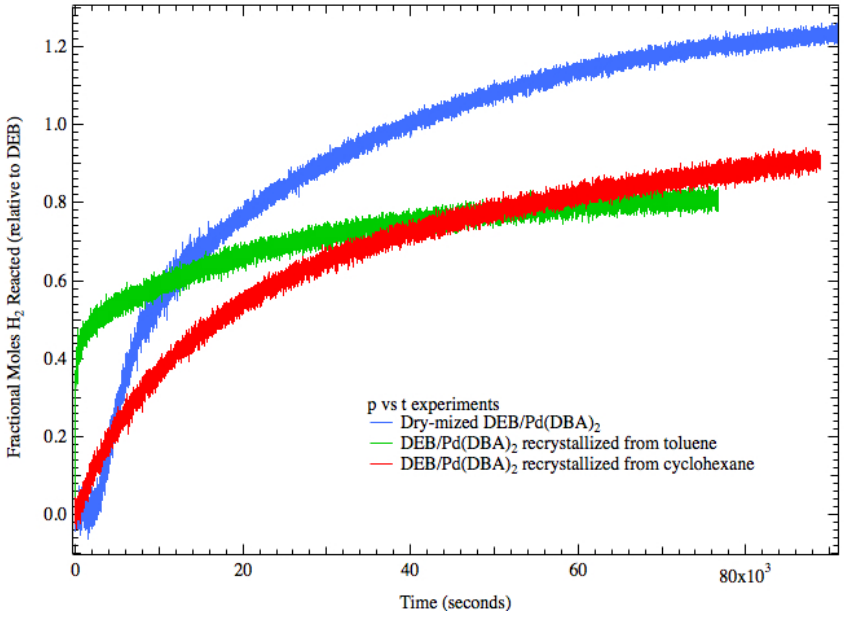

Figure 3-5: Reaction vs. time data for the three reference blends of DEB and Pd-dba.

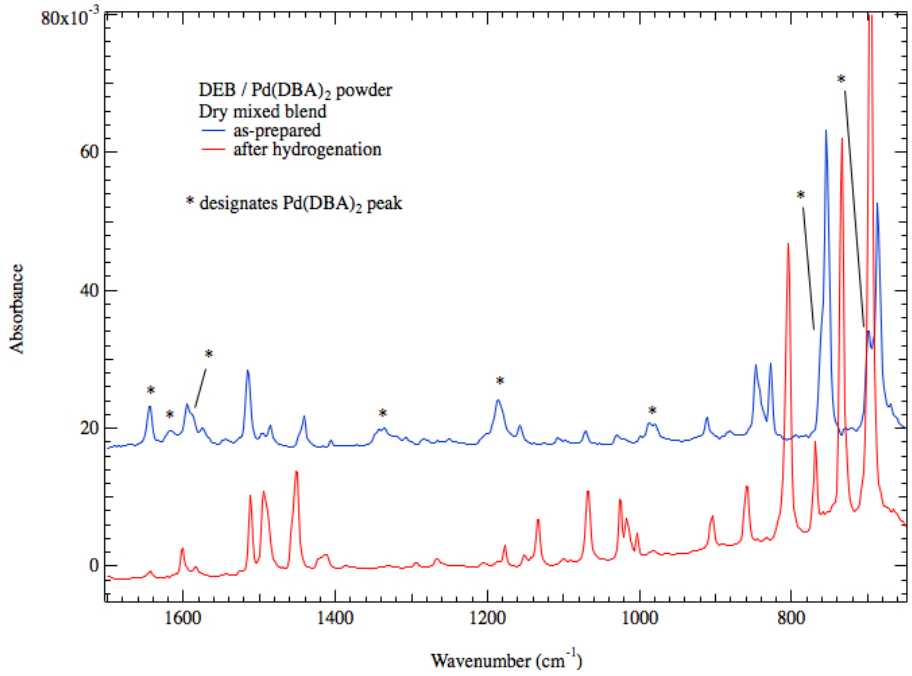

Figure 3-6: IR absorption spectra for the dry-mixed DEB/Pd-dba blend, before and after hydrogenation.

The extra getter capacity provided by the dba ligands is potentially beneficial. However, it is necessary to consider the possibility of the production of volatile compounds during hydrogenation. Such compounds would not represent a pressurization hazard – the net change in moles of gas during reaction with hydrogen would still be negative. However, they might have a negative impact on long-term material stability and compatibility. In this case, given the structure of the dba ligand, the significant formation of volatile species is unlikely. Furthermore, the experimental data do not support such a possibility. The formation of volatile species would partially mask the measured drop in pressure as hydrogen is removed from the closed test system. This is turn would have the effect of lowering the calculated extent of reaction. Since the reaction was calculated to proceed to nearly 95% on the basis of all organic content, this can not have been a large effect. Furthermore, the measured mass gain of the sample upon hydrogenation was found to be consistent, within experimental uncertainty, with the formation of only non-volatile products. More detailed experiments will be performed in the future to confirm this.

The data presented in Fig. 3-5 show that hydrogenation of DEB/Pd-dba recrystallized from toluene is extremely rapid in comparison to the dry-mixed sample. This suggests intimate mixing of the getter and catalyst, as would be expected for preparation from a true solution. However it is interesting that the calculated extent of reaction (based on DEB content) is only 85%. This in turn suggests that the dba ligands contribute little or nothing to the overall getter capacity.

IR absorption data partially explain this observation, but raise other questions. Spectra are shown in Figure 3-7 for DEB/Pd-dba recrystallized from toluene (and cyclohexane), as well as for the dry mixed blend. The absorption features attributed to Pd-

dba are marked with asterisks. Consistent with the reaction data, these features are almost entirely absent from the toluene-based sample. Literature reports indicate that solutions of Pd_2DBA_3 in toluene or chloroform can form complexes of the type Pd_2DBA_3(solvent) [5,6]. These complexes slowly decompose to form Pd nanoparticles. It is therefore possible that the material recrystallized from toluene may contain a high concentration of Pd nanoparticles. This is consistent with the color of the material. Whereas the dry-mixed blend retains the dark purple color of pure Pd-dba, the material recrystallized from toluene is grey, with only a very faint purple tint. However the IR and hydrogenation data suggest a virtual lack of DBA in any form in the mixture. Free DBA is a non-volatile compound with a boiling point of 130˚C. It should therefore remain in the sample during the solvent evaporation step, and should be evident from its bright yellow color. Furthermore, it seems extremely unlikely that a DBA-toluene complex would be volatile, and so the DBA should not have been removed in this form either. Further experiments will be required in order to understand these results.

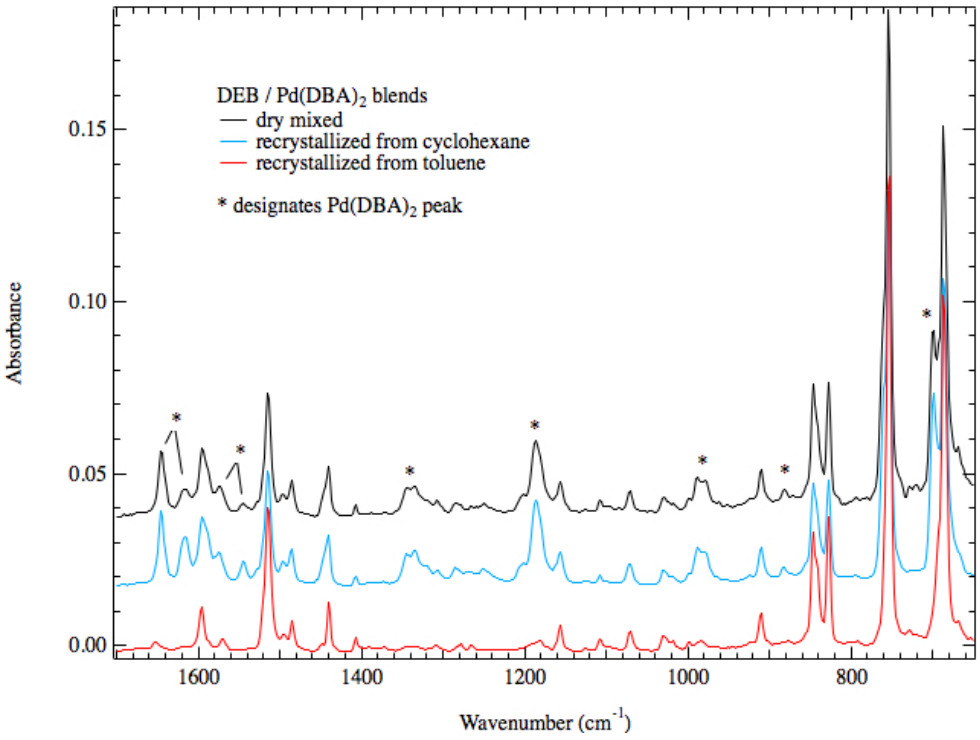

Figure 3-7: IR absorption data for DEB/Pd-dba blends recrystallized from toluene and cyclohexane, as well as for the dry mixed blend.

Next consider the behavior of the DEB/Pd-dba blend recrystallized from cyclohexane. The IR absorption spectrum for this blend, shown above in Fig.3-7, is virtually identical to that of the dry mixed blend. Specifically, the absorption features attributed to Pd-dba are unaltered, suggesting that it is present in the recrystallized material in the expected concentration. The color of the blend supports this observation. It appears purple/grey/brown – much more similar to the dry mixed blend than to the material recrystallized from toluene.

Hydrogenation data for the cyclohexane-based blend are shown as a function of time in Fig. 3-5. The reaction is seen to proceed rather slowly, suggesting relatively poor mixing of the getter and catalyst. This is consistent with recrystallization from a suspension rather than from a true solution. There is likely strict segregation of the DEB and Pd-dba crystallites, resulting in relatively large spatial separation between the getter and catalyst.

Extrapolation of the data provides a reaction extent of 101% with respect to DEB content, intermediate between the dry mixed and toluene-based blends. If the DEB is assumed to react to 95%, it can be estimated that approximately 32% of the Pd-dba present also underwent hydrogenation, a much lower percentage than was observed for the dry mixed blend. The relative lack of DBA hydrogenation is confirmed by the IR absorption data shown in Figure 3-8. It can be seen that there is only a small decrease in absorption from DBA after hydrogenation. This too is consistent with visual observation. The dry mixed blend is essentially black in color after hydrogenation. However, the blend recrystallized from cyclohexane is distinctly reddish, retaining significant color from the Pd-dba. The reason for the difference in extent of reaction is unknown. If there is very poor mixing of the getter and catalyst, the relative lack of DBA hydrogenation may be related to the incubation period and very slow reaction rate observed for pure Pd-dba. Further study will be required in order to explain these observations.

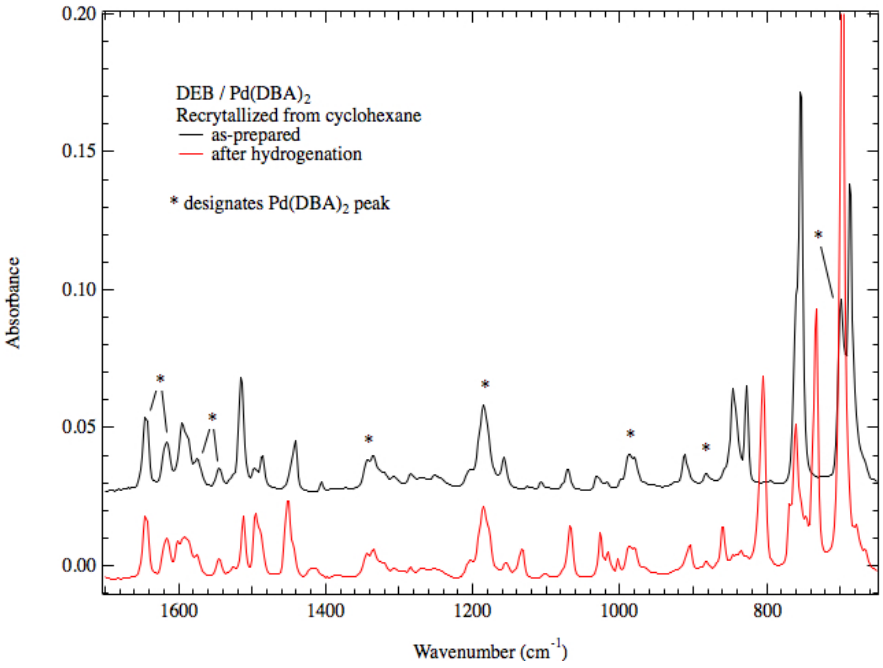

Figure 3-8: IR absorption spectra for the DEB/Pd-dba blend recrystallized from cyclohexane, before and after hydrogenation.

3b: Results – Infiltrated Foams

Reaction vs. time data are shown in Figure 3-9 for a getter-infiltrated foam sample prepared from toluene. Also shown for comparison are the corresponding data for

DEB/Pd-dba powder recrystallized from toluene solution. The initial reaction rate is notably slower for the infiltrated foam. This suggests that some getter/catalyst segregation occurs during solvent evaporation. It is not unreasonable to suppose that such segregation would have a greater impact for the quasi two-dimensional structure of the infiltrated deposit than it would for a bulk powder sample.

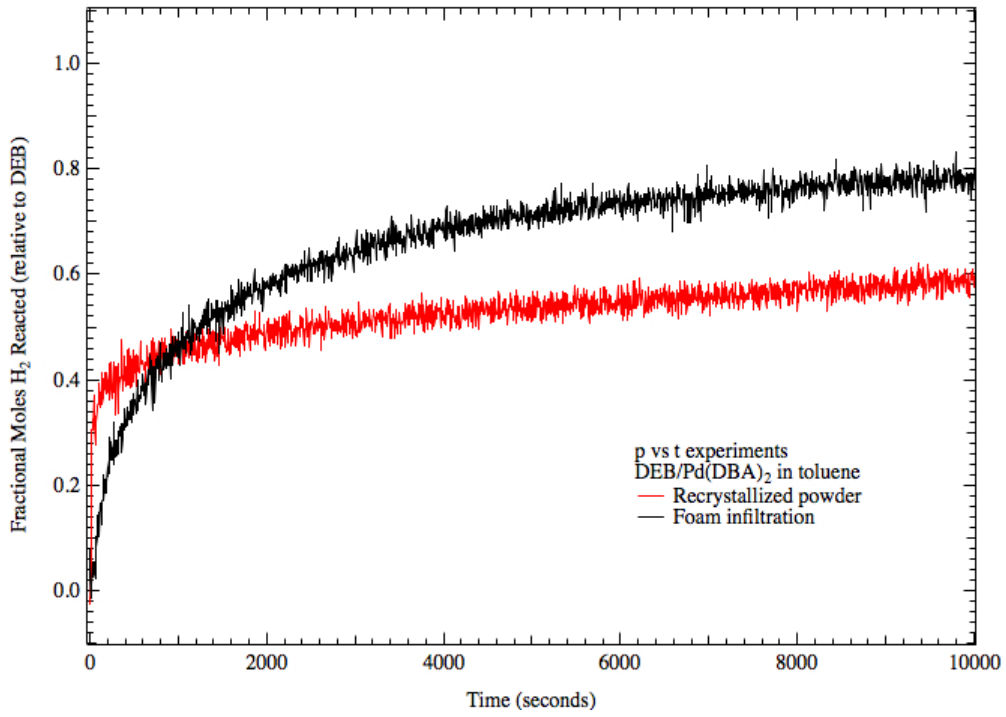

Figure 3-9: Reaction vs. time data, normalized to DEB content, for a getter infiltrated foam prepared using a toluene solution. Also shown are the corresponding data for DEB/Pd-dba powder recrystallized from toluene.

The extent of reaction for the infiltrated sample is calculated to be 81% with respect to the DEB content. This is similar to the result obtained for the recrystallized powder sample. The physical appearances of the infiltrated and powder samples are likewise similar – dark grey with no purple tint. These observations suggest the presence of Pd nanoparticles, and little DBA, in the infiltrated sample. However, IR absorption data do not support this conclusion. Absorption spectra are shown in Figure 3-10 for the infiltrated sample, before and after hydrogenation. Also shown are data for the corresponding recrystallized powder before hydrogenation. The absorption data clearly show the presence of Pd-dba in the infiltrated getter deposit, and confirm that it has reacted to a considerable extent during hydrogenation. One can recalculate the extent of reaction with respect to the DEB + DBA content using the nominal composition of the deposit. The result is a value of 67%.

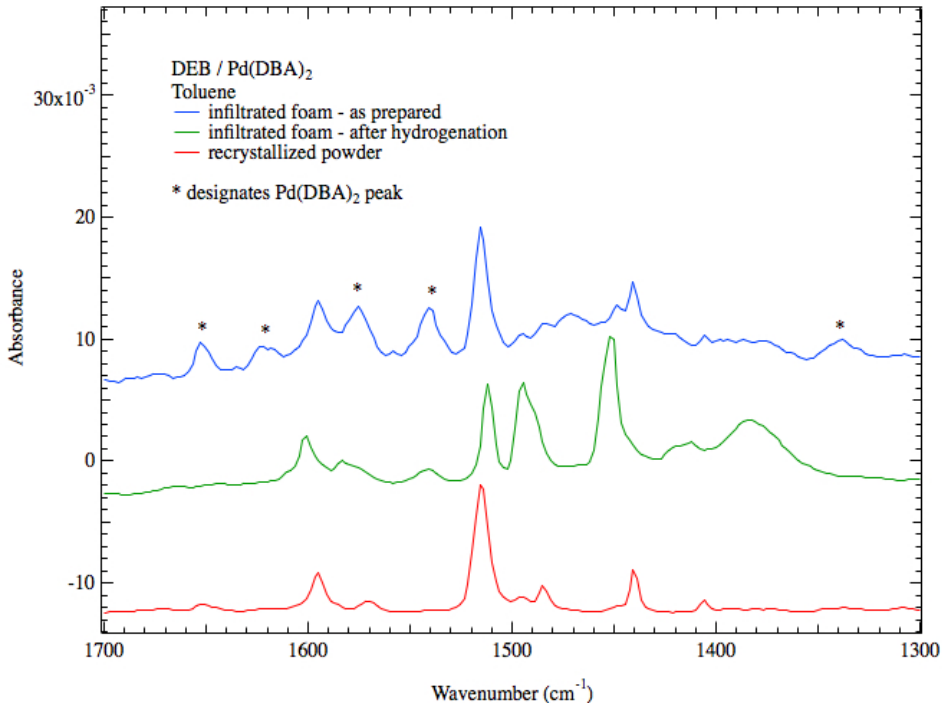

Figure 3-10: IR absorption data for the getter-infiltrated foam sample prepared from toluene, before and after hydrogenation. Also shown are data for the corresponding recrystallized powder before hydrogenation.

The hydrogenation vs time data for the toluene-based infiltrated sample are replotted in Figure 3-11. Also shown are the corresponding data for samples prepared from ethanol and cyclohexane suspensions. Hydrogenation of the sample prepared from cyclohexane is very slow, and only proceeds to 40% with respect to DEB content. The physical appearance of this sample is very similar to that of the corresponding recrystallized powder – greyish purple in color – suggesting a significant concentration of intact Pd-dba. This is confirmed by the IR absorption data presented in Figure 3-12. The spectra for the infiltrated deposit and recrsytallized bulk powder are virtually identical, with strong absorption features from Pd-dba. Also, it is clearly seen that the Pd-dba present in the infiltrated deposit undergoes little/no reaction upon hydrogen exposure.

For cyclohexane, the properties of the infiltrated deposit and the corresponding recrystallized powder, are qualitatively very similar. Quantitatively, as with the toluene-based samples, the infiltrated material reacts with hydrogen more slowly and to a lesser extent. In each case this can probably be attributed to the segregation of getter and catalyst crystals that occurs solvent evaporation, exacerbated by the quasi two-dimensional nature of the infiltrated deposit.

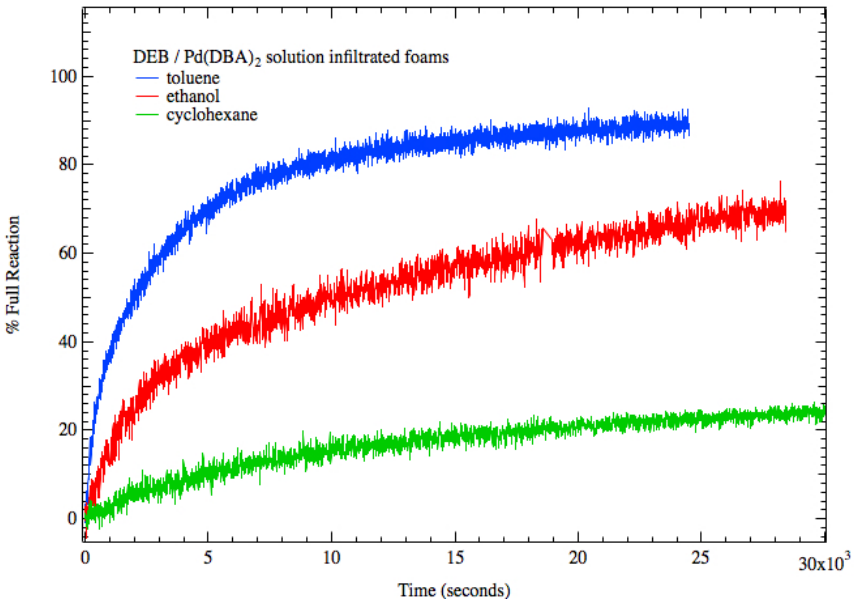

Figure 3-11: Hydrogenation vs. time data for getter-infiltrated foam samples prepared using toluene, ethanol, and cyclohexane. The data are normalized with respect to the DEB content only.

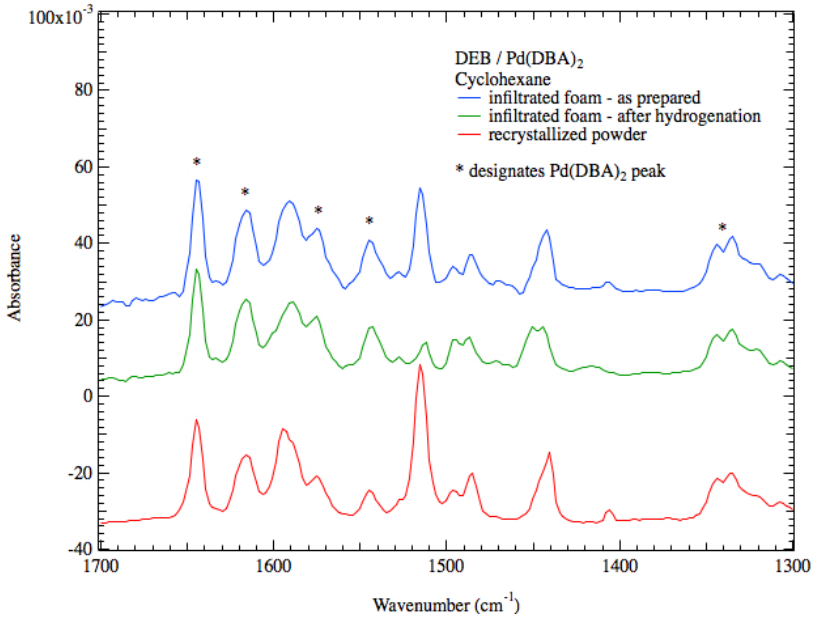

Figure 3-12: IR absorption data for the getter-infiltrated foam sample prepared from cyclohexane, before and after hydrogenation. Also shown are data for the corresponding recrystallized powder before hydrogenation.

Finally, intermediate behavior is observed for the hydrogenation of infiltrated samples prepared using ethanol. The infiltrated foam appears mostly grey in color, but with some purplish areas interspersed. This suggests a non-uniform distribution of Pd nanoparticles and intact Pd-dba. The hydrogenation proceeds to 87% with respect to DEB content, very close to the result for the toluene-based sample. However the reaction rate is considerably lower, suggesting less intimate mixing of getter and catalyst. This would be expected based on preparation from a suspension, rather than a true solution. However, the degree of getter/catalyst segregation is presumably not as great as observed for the cyclohexane-based sample.

The hydrogenation rate of a getter composite will depend on the degree of getter/catalyst mixing. Mixing at a truly molecular level would be expected to lead to very fast reaction. However if, as the solvent evaporates, one component comes out of solution much earlier than the other (or does not fully dissolve in the first place), than significant segregation of the getter and catalyst may occur. The hydrogenation reaction relies on the diffusion of atomic hydrogen from the catalyst site to an unsaturated DEB molecule. Significant segregation of the two components may therefore limit the reaction rate and even the total extent of reaction. Elemental maps prepared using SEM/EDS are a useful means of studying getter/catalyst segregation. Figure 3-13 shows a comparison of C and Pd maps measured for getter-infiltrated foams prepared using toluene and ethanol. Within the limited sampling area, the ethanol-based sample contains numerous surface grains containing both C and Pd, suggesting the presence of crystalline Pd-dba segregated from the getter deposit. In contrast, both C and Pd are more uniformly distributed within the toluene-based sample. This suggests overall more intimate mixing of the getter and catalyst, and is consistent with the much higher reaction rate for the toluene-based material.

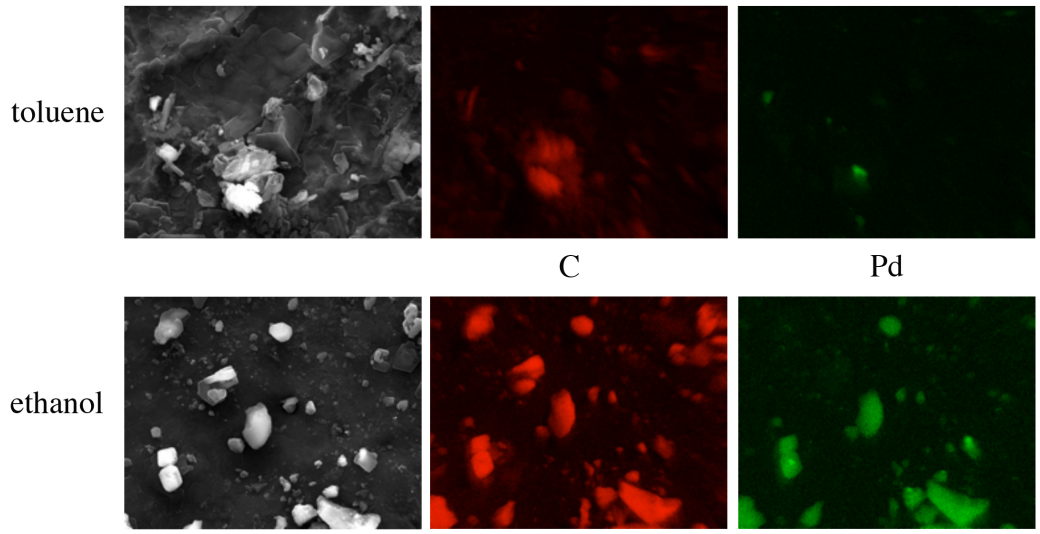

Figure 3-13: SEM images and EDS elemental maps for getter-infiltrated foams prepared using toluene and ethanol.

Additional examples of comparative SEM imagery are shown in Figures 3-14 and 3-15. For the sequence of toluene – ethanol – cyclohexane it can be seen that a progressively larger fraction of the getter deposit is in the form of discrete grains on the foam surface, rather than a uniform film. This is fully consistent with the progressively lower performance measured for this sequence of samples. This does suggest that toluene is the solvent of choice among those studied for solution deposition. However, it will clearly be necessary to perform additional experiments in order to better understand the behavior and role of Pd-dba in this case.

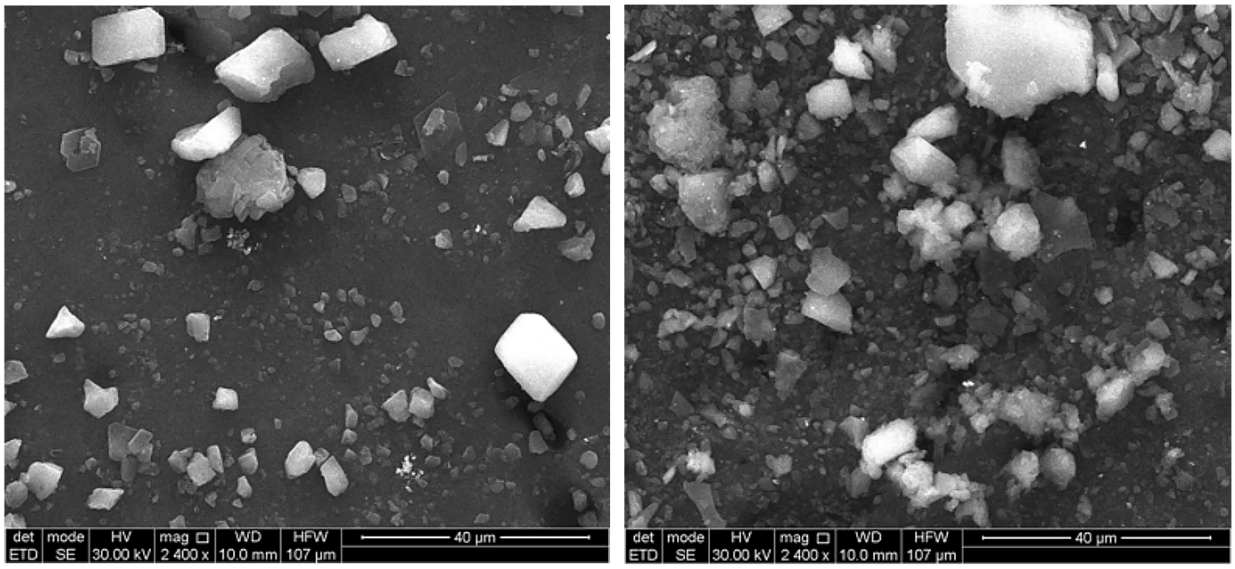

ethanol cyclohexane

Figure 3-14: SEM images for getter-infiltrated foams prepared using ethanol and cyclohexane.

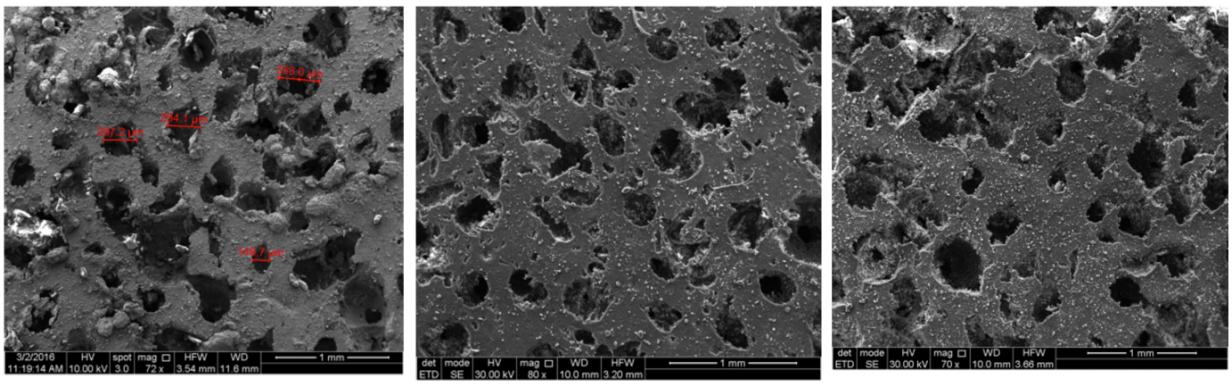

toluene ethanol cyclohexane

Figure 3-15: SEM images for getter-infiltrated foams prepared using toluene, ethanol and cyclohexane.

It is of interest to compare the performance of the toluene-based materials to that of the standard DEB/Pd/C composite produced at KCNSC. Reaction vs. time data for these materials are shown in Figure 3-16. The performance of DEB/Pd-dba powder recrystallized from toluene is found to be essentially equivalent to that of the DEB/Pd/C baseline. This confirms that dissolution in and recrystallization from toluene do not damage the structure of DEB, nor the catalytic activity of the Pd-dba. The initial hydrogenation rate is found to be lower for getter-infiltrated foams. This suggests that the recrystallization of DEB/Pd-dba under inhomogeneous conditions to form a quasi two-dimensional film provides less intimate mixing of the getter and catalyst.

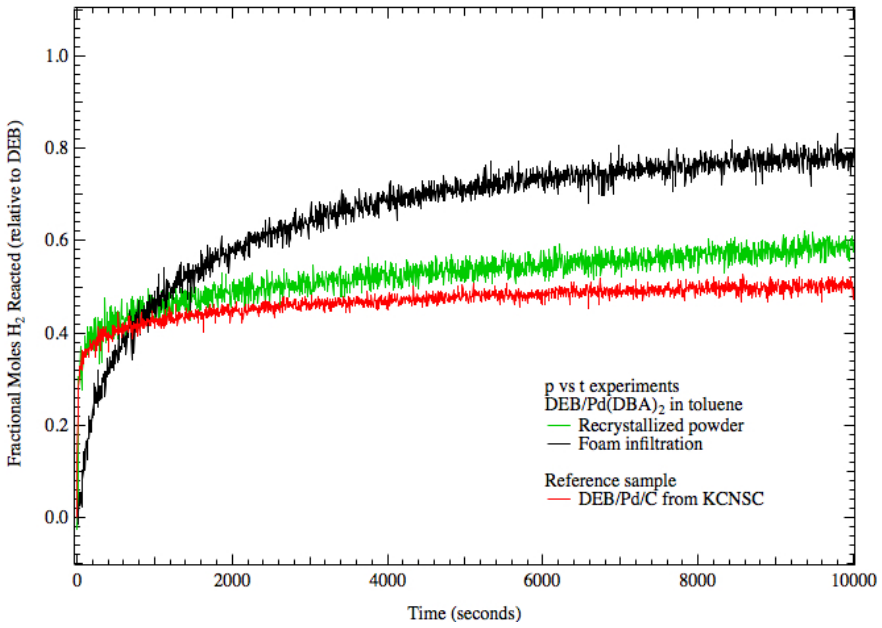

Figure 3-16: Hydrogenation vs. time data for toluene-based samples and for the standard DEB/Pd/C material prepared at KCNSC.

One concern regarding the use of toluene for solution infiltration is the potential for degradation of mechanical properties caused by swelling and the removal of unpolymerized resin. As an initial evaluation, load-displacement tests were performed on un-infiltrated M9763 silicone samples. Five 1" diameter samples were cut from 1 mm thick foam sheet. These were placed in pure toluene, with magnetic stirring, for 27 hours. The foams were then removed and the toluene evaporated under ambient conditions. Five control samples of the same size were also prepared. The load-displacement tests were performed on an MTS Insight 30 using a 1 kN load cell. For each sample three loading/unloading cycles were performed at a displacement rate of 1.27 mm/min, with load data taken up to 60% displacement. Some sample-to-sample variation was observed. Figure 3-17 shows the upper and lower ranges of the resulting data for both the toluene-exposed and control samples. It is found that toluene exposure does decrease the stiffness of the silicone foam by approximately 11%, which does appear to be statistically significant with respect to the sample-to-sample variation. However, the degradation is not sufficient

to disqualify solution infiltration for this application. Future work will examine compression set, additional foam types, and the effects of infiltration/hydrogenation.

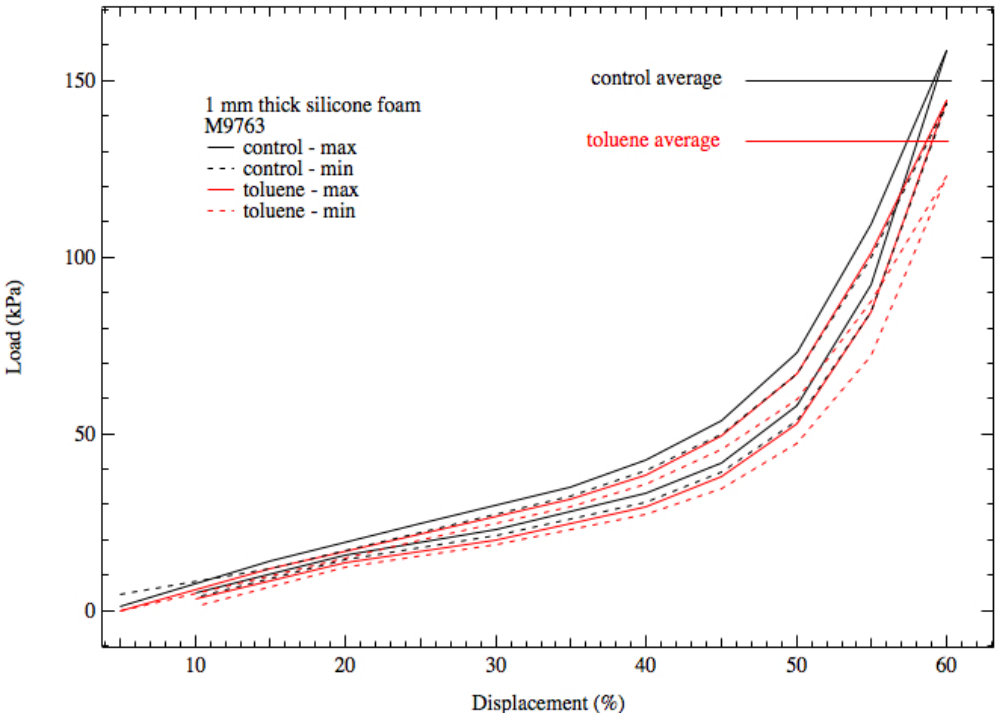

Figure 3-17: Load-displacement data for control samples, and for samples exposed to pure toluene for 27 hours.

4: Vapor Deposition

4a: Experimental Procedure

The vapor deposition system as it was configured at the start of FY16 is shown schematically in Figure 4-1. It consists of a box-shaped vacuum chamber equipped with a mechanical roughing pump and control system that provides an operating pressure that is typically in the range of 0.1-1 Torr. Separate sublimation/evaporation sources for the getter and catalyst are mounted at the base of the chamber, along with an inlet for argon carrier gas that aids transport of the precursor vapors to the substrate. These sources are filled with fresh precursor material before each run, in order improve process control and run-to-run reproducibility. Two general substrate configurations are available. Films can be deposited onto flat substrates using a conventional mount, or infiltrated into open-celled porous materials using a forced-flow configuration. In either case the substrates could be illuminated with UV radiation from mercury vapor lamps, in order to modify the deposition chemistry if desired. There were, however, several problems associated with the use of mercury vapor lamps:

1) They provide only a low power density, about 1 mW/cm^2 at the substrate;

2) A complex arrangment is needed in order to prevent film deposition onto the lamps, which would degrade effective output and lifetime;
3) The lamps represent a health hazard in the event of breakage.

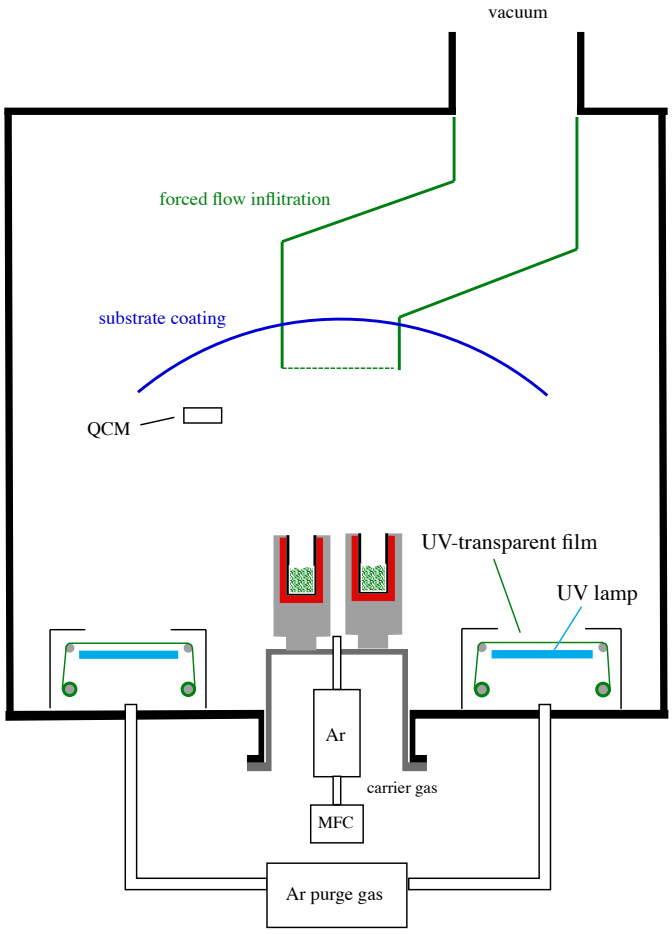

Figure 4-1: Schematic illustration of the vapor deposition system as it was configured at the start of FY16.

Because of the issues associated with mercury vapor lamps, it was decided to investigate the use of UV LED systems as an alternative. Currently available UV LEDs are capable of providing high total power, and eliminate the health hazards of mercury. The disadvantage of UV LEDs, however, is that they are not capable of irradiating large areas at high power density. For this reason it was decided to use a collimated LED to irradiate only the vapor plume directly above the Pd evaporation source, rather than the entire substrate. This configuration is also much more suitable for use in a scaled-up system coating larger and/or more numerous substrates.

Figure 4-2 shows photographs of the LED chip and collimation lens assembly used for this purpose. The output spectrum of the LED is shown in Figure 4-3. It peaks at a wavelength of 365 nm, which corresponds to a photon energy of 3.4 eV. The collimation

assembly is capable of providing a 1" diameter beam with a power density of 25-30 mW/cm^2. The photon energy and power density are sufficient for the study of UV-assisted deposition.

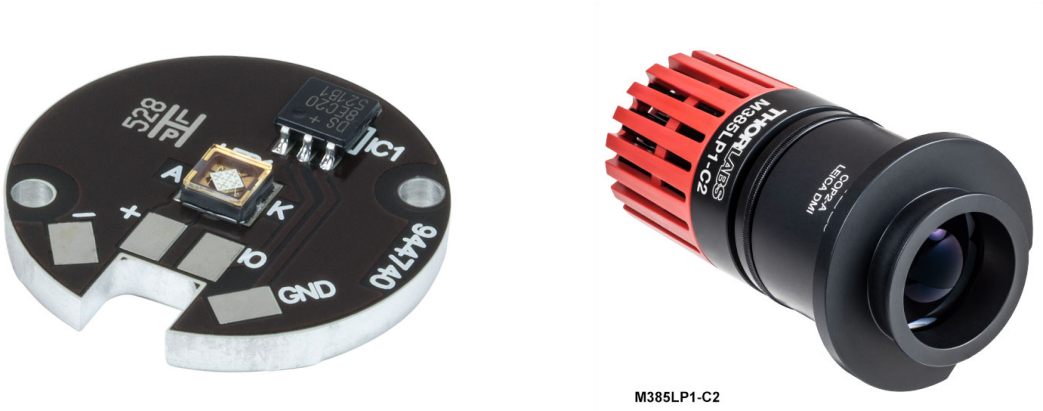

Figure 4-2: Photographs of a typical high-power UV LED (left), and the LED/lens system used for the vapor deposition experiments (right) [7].

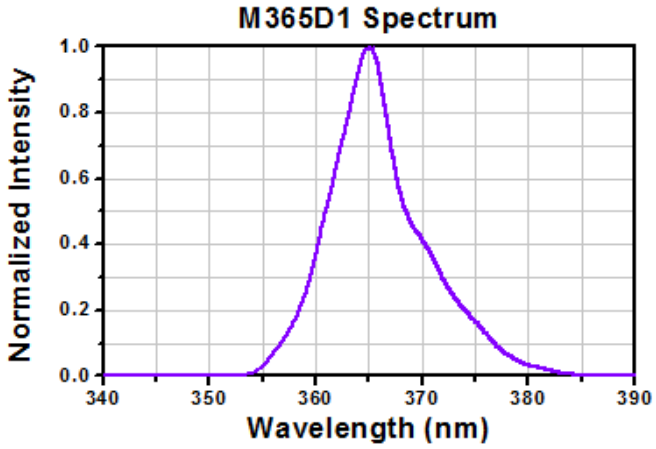

Figure 4-3: Spectral output of the 365 nm UV LED used for the vapor deposition experiments [7].

The configuration of the modified deposition system is shown schematically in Figure 4-4. Initial experiments were performed with the LED assembly mounted within the vacuum chamber. However the lack of convective cooling under vacuum severely limited the LED lifetime. The assembly was therefore mounted externally to the chamber, with the beam passing through a fused-quartz vacuum viewport. As seen from the data presented in Figure 4-5, the transmission of this viewport at 365 nm is approximately 90%. Replacement of this window with UV glass would enable the use of a shorter wavelength LED with greater photon energy. This may be considered for future work. Finally, note

that the viewport is recessed several inches from the main portion of the deposition chamber. Nevertheless some material is deposited onto the inner surface over the coarse of a run, which reduces the intensity of the UV beam by approximately 25%. A gas curtain will be added to the system in the future in order to reduce/eliminate deposition onto the window.

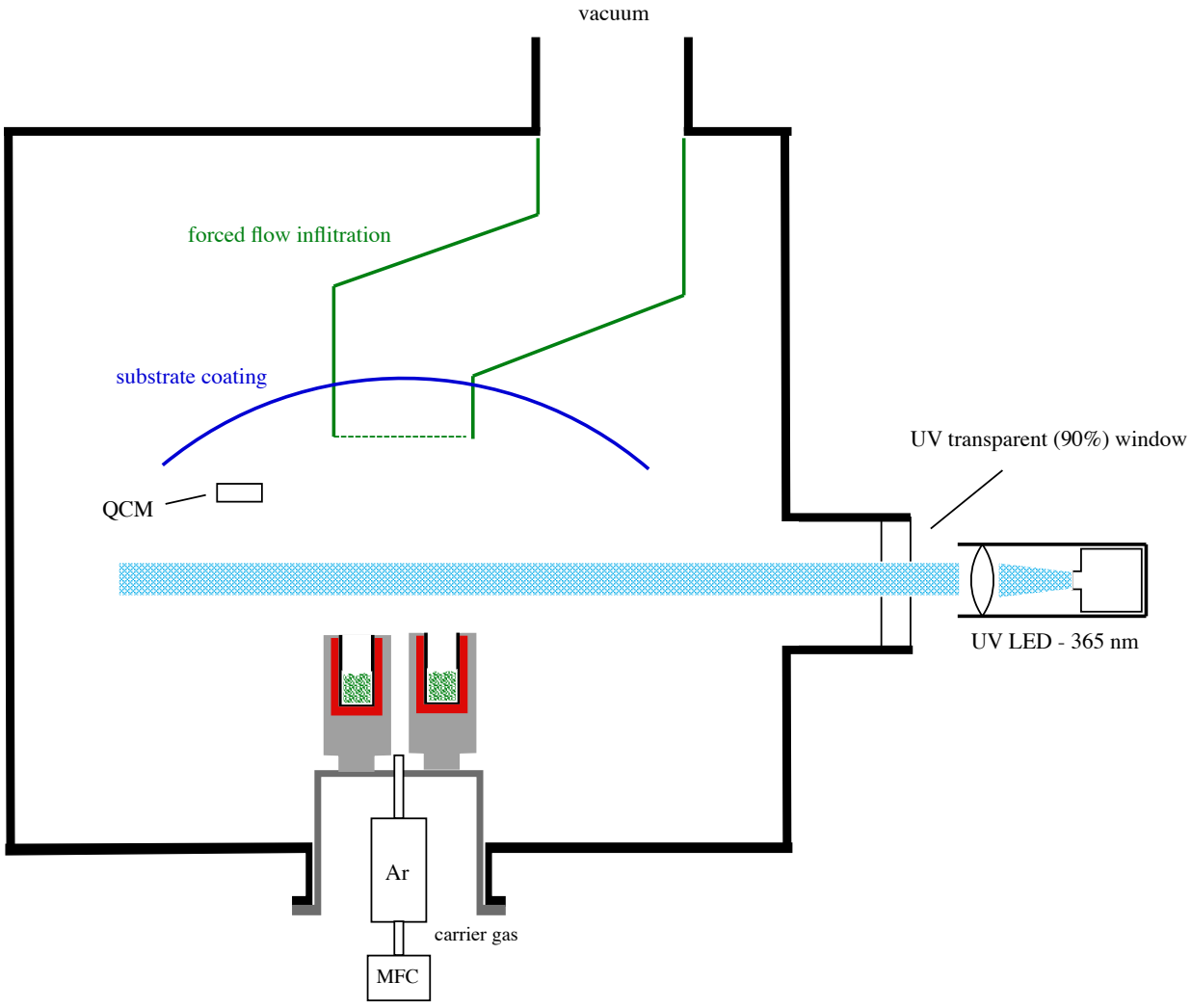

Figure 4-4: Schematic illustration of the vapor deposition system in its latest configuration.

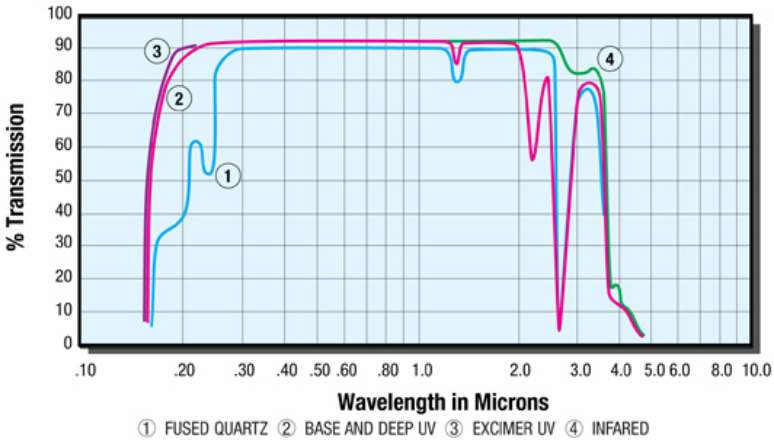

Figure 4-5: Transmission vs. wavelength data for several type of vacuum viewports [8].

4b: Pure cp-Pd-pp

The Pd precursor used for vapor deposition of the getter/catalyst composite is cyclopentadienyl[(1,2,3-n)-1-phenyl-2-propenyl]palladium, or cp-Pd-pp, which has the structure shown in Figure 4-6. Work performed in FY15 demonstrated that this compound in its pristine form is already catalytically active with respect to the dissociation of molecular hydrogen – reduction of the Pd to its metallic state is not required. Furthermore, the organic ligands were found to readily react with hydrogen under the conditions tested. Hydrogenation and mass loss data imply complete reaction of the ligands to propylbenzene and volatile cyclopentane. The generation of volatile species is not a concern with respect to pressure build-up, as the net change in gas-phase moles upon hydrogen would still be negative. However, the gas would be free to migrate throughout the closed system and may lead to material stability or compatibility issues.

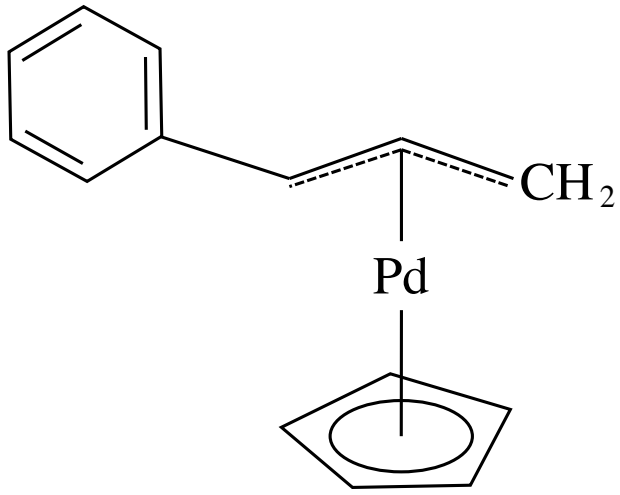

Figure 4-6: Molecular structure of the Pd organometallic compound cyclopentadienyl[(1,2,3-n)-1-phenyl-2-propenyl]palladium, or cp-Pd-pp.

FY15 data also showed that vapor deposited cp-Pd-pp could act as a getter, but little was done to investigate the details of the reaction. For FY16 vapor deposited samples were prepared in order to:

1) determine the structure of the deposited material as compared to the starting material;
2) determine the degree of hydrogenation;
3) determine if volatile species are created during hydrogenation and, if so, identify them if possible;
4) determine the effect of UV exposure during deposition on all of the above.

Infiltrated samples were prepared in the forced-flow mode using M9777 silicone foam substrates prepared at KCNSC. This foam has a thickness of 1 mm and a nominal porosity of 77%. The substrates were 3" diameter circles, and typical deposition conditions provided a loading of 15-20 mg of cp-Pd-pp per deposition run. Samples were also prepared on a variety of other materials using the conventional substrate mounting geometry.

Hydrogenation Behavior

Initial experiments examined the hydrogenation behavior of vapor infiltrated cp-Pd-pp. The influence of UV exposure during deposition was evaluated using a 23 mW/cm^2 beam directed through the vapor plume, as described in the previous section. The fractional extent of reaction was calculated assuming that each mole of cp-Pd-pp has the potential to react with four moles of H_2. The resulting data for hydrogenation as a function of time are presented in Figure 4-7. Within experimental uncertainties, the data for all of the samples are equivalent with respect to both reaction rate and extent – UV exposure has no significant influence on the gettering behavior of the deposit. The average extent of reaction is calculated to be 85.0%, or 3.40 mole H_2/mole cp-Pd-pp. This suggests, but does not prove, that the cp-Pd-pp is deposited substantially intact. Significant loss of either cp or pp ligands during deposition would leave insufficient organic material to account for the observed reaction. It is possible, however, that the ligands do dissociate from the Pd atom during heating/evaporation, but are still deposited approximately stoichiometrically within the growing film.

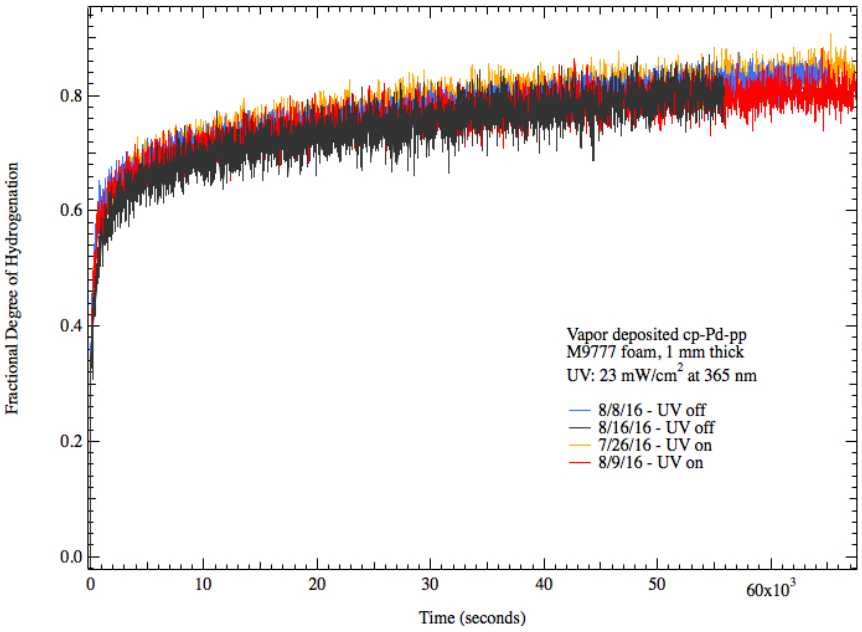

Figure 4-7: Hydrogenation vs. time data for samples vapor infiltrated with pure cp-Pd-pp.

All of the samples were found to lose mass during hydrogenation, implying the formation of volatile species. However, it should first be noted the samples were stored under ambient conditions in the time between deposition and testing, typically overnight. They were found to gain mass during this time, typically about 5.3% with respect to the mass of deposited material. The mass gain was accompanied by a change in color from pinkish-brown to drak reddish-brown, suggesting reaction with ambient oxygen. The samples were then found to *lose* mass during hydrogenation, on average 14.2% with respect to the mass of material originally deposited. The implied formation of volatile species would skew the pressure vs. time data, masking some of the pressure loss and leading to an artificially low calculated extent of reaction. Assuming that the mass loss is primarily due to the formation and volatilization of cyclopentane, it is possible to estimate a corrected extent of reaction. The result is a value of 95-100%, consistent with the intact deposition and near complete hydrogenation of the cp-Pd-pp.

Subsequent to hydrogenation, IR gas cell and residual gas analysis (RGA) measurements were performed in an effort to identify the volatile species. These were fairly crude proof-of-principle tests, designed to evaluate the suitability of the methods for this purpose. Note also that comparison data were not taken for samples before hydrogenation, so it can not be stated with certainty that any species detected were not present in the as-deposited state. Nonetheless the results were interesting, and more sophisticated tests will be performed in the future. For the IR measurement, a hydrogenated foam sample was placed at the bottom of a gas cell, and the cell was placed in the path of the IR probe beam. In this case one of the samples prepared with UV exposure of the vapor plume was chosen. The gas cell was not evacuated, nor even equipped with windows. Nonetheless the spectrum shown in Figure 4-8 clearly shows absorption features from volatilzed species. The absorption seen in the range of 3400-3800 cm^{-1}

indicates the presence of both bound and free –OH groups. This is consistent with the theory that the as-prepared samples reacted with ambient oxygen during overnight storage. In addition, a number of features are seen in the range of 500-1000 cm^{-1}. No pattern can be discerned from this admittidly crude data, but the features are consistent with the presence of aromatics, C5 rings, olefinic chains, or some combination of each. It is therefore not possible to state if the volatile species are derived from the cp ligands, the pp ligands, or both. This question will be examined in the future with more rigourous experiments.

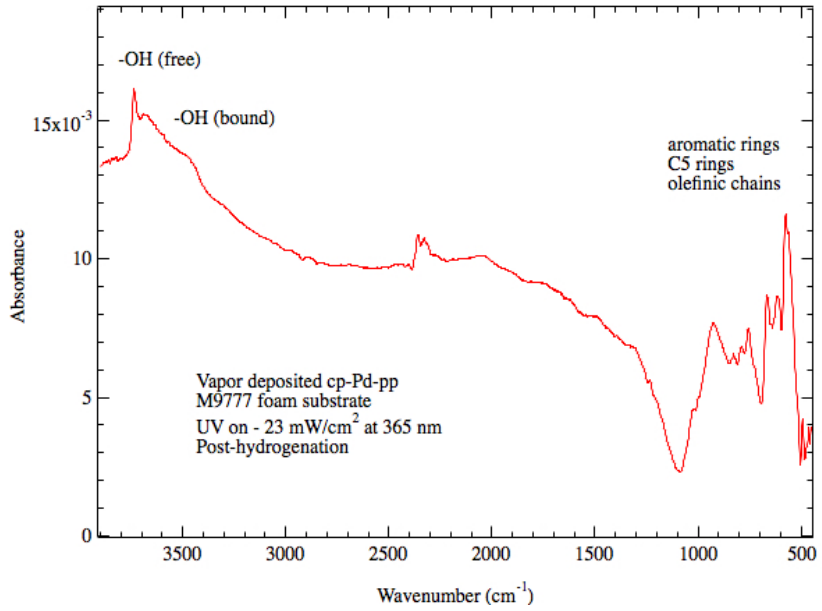

Figure 4-8: IR absorption spectrum of volatile species liberated from a sample of hydrogenated, vapor deposited, cp-Pd-pp.

The second of the proof-of-principle experiments used a Stanford Research Systems residual gas analyzer to obtain mass spectra of the volatilized species. The sample to be tested was placed in a vacuum chamber directly below the RGA inlet. The chamber was evacuated to a pressure of $1x10^{-5}$ Torr before beginning the measurement, and residual gas in the mass range of 1-200 amu was analyzed. Samples prepared both with and without UV exposure were tested, and background data were also obtained with no sample in place. The mass spectra obtained after background subtraction are shown in Figure 4-9. Numerous C3-C10 species are detected at various levels of hydrogenation. It is likely that oxygenated species are also present, but these can not be deconvoluted from the CH_n species. For reference, recall that the cp ligand is a C5 molecule, and the pp ligand is C9. No effort was made to fit the mass spectra in detail. However, a number of reference spectra obtained from the NIST webpage were examined [9]. Figure 4-10 shows reference data for cyclopentane and propylbenzene, the fully hydrogenated forms of the cp and pp ligands, respectively. The data obtained from the hydrogenated samples are broadly consistent with the presence of both of these compounds – in other words the volatile species do not appear to be uniquely derived from either the cp or pp ligands. This is again consistent

with the theory that cp-Pd-pp is deposited largely intact. Finally, note that there are no dramatic differences observed between the samples prepared with or without UV exposure. This suggests that the UV flux and/or photon energy are not sufficient to cause significant dissociation of the cp-Pd-pp vapor. As with the IR gas cell, more rigorous experiments will be performed in the future.

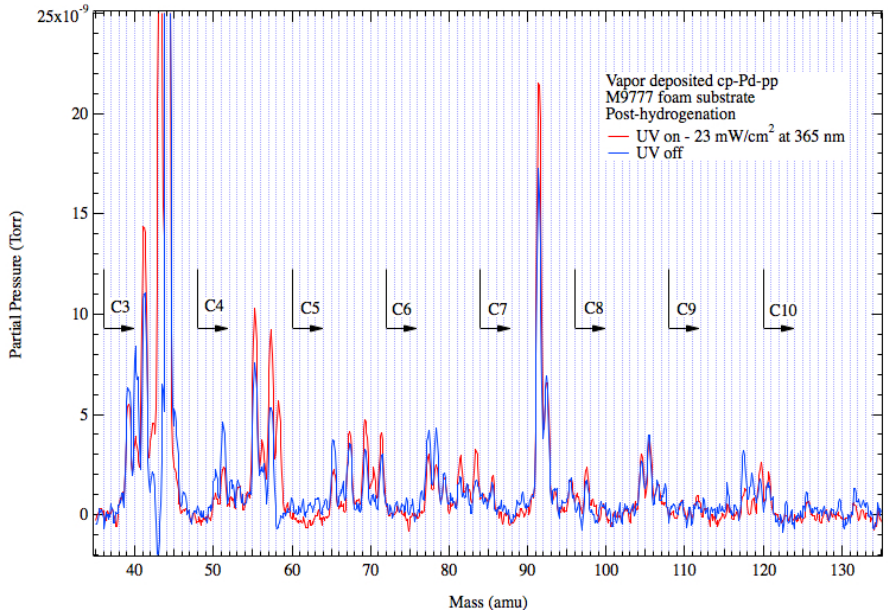

Figure 4-9: RGA mass spectra of the volatile species liberated from hydrogenated, vapor deposited, cp-Pd-pp samples. Data are shown for material produced both with and without UV exposure.

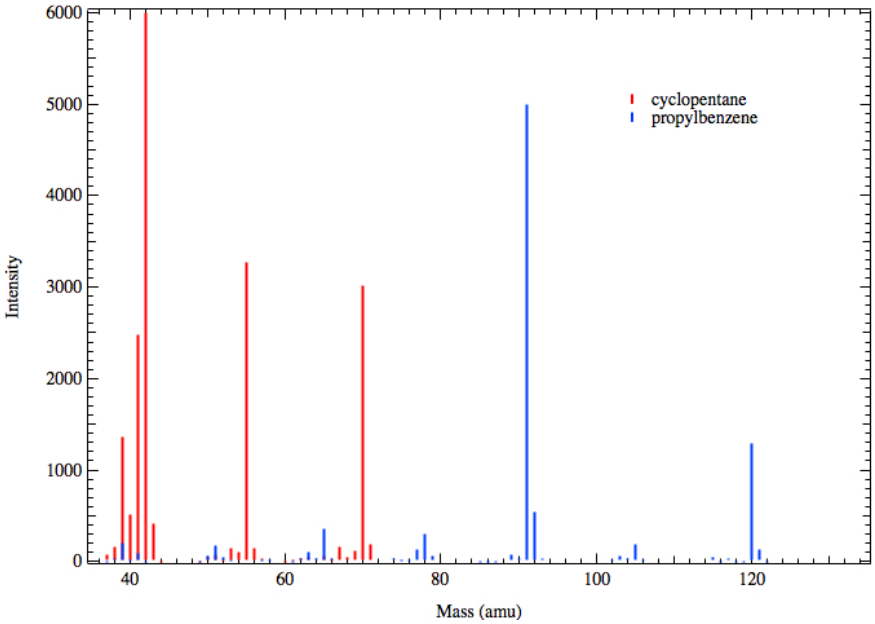

Figure 4-10: Reference RGA data for cyclopentane and propylbenzene [9].

Composition/Structure Determination

A number of experiments were performed in an effort to more directly measure the structure of vapor-deposited cp-Pd-pp. During the deposition of cp-Pd-pp there is a competition between the sublimation/evaporation of material from the source, and thermal decomposition of the material remaining in the source. In a typical run approximately 50% by mass of the precursor is volatilized. The remainder forms a non-volatile gummy black compound. The first experiment in this series was to examine the composition and structure of the residue.

To measure the residue composition, a portion of the gummy material was painted onto a carbon substrate for Rutherford backscattering analysis. Backscattering spectra were obtained at the LANL Ion Beam Materials Lab using a 2 MeV He^+ beam, and a scattering angle of 167°. The energy spectrum of backscattered ions is shown in Figure 4-11. Analysis of the spectrum provides a composition of $Pd_1C_{9.0}O_{0.93}$. It is likely that the oxygen in the sample is the result of reaction with ambient air after the material was removed from the deposition system. The overall composition of cp-Pd-pp is $PdC_{14}H_{14}$, with the cp ligand being C_5H_5 and the pp ligand C_9H_9. This suggests two possibilities:

1) the residue is primarily composed of a Pd complex with the pp ligand – that is, the mechanism of thermal decomposition is primarily the loss of the cp ligand;
2) decomposition causes the loss of both cp and pp in an unknown ratio to result in an overall composition of Pd/C ~ 9.

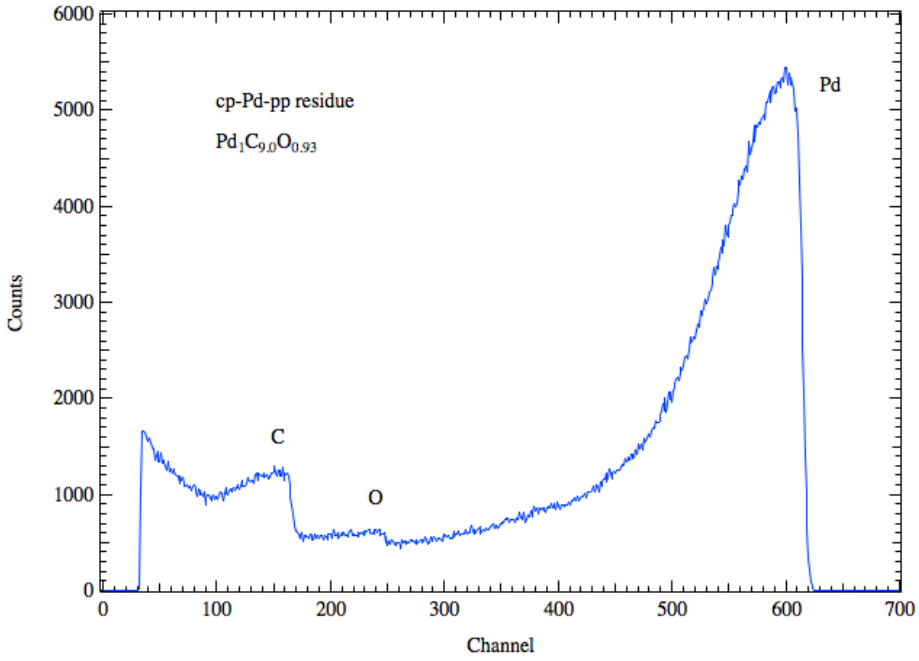

Figure 4-11: Rutherford backscattering data for the cp-Pd-pp residue created by thermal decomposition during a deposition run.

These two options can be resolved by determining the structure of the residue. The IR absorption spectrum for the residue is shown in Figure 4-12. Reference data for the cyclopentadiene and phenyl-2-propanyl ligands are also shown. The results strongly

suggest that the residue is composed primarily of the pp ligand. This supports the theory that thermal decomposition of cp-Pd-pp occurs primarily through the loss of cp, leading to the formation of a non-volatile Pd-pp complex.

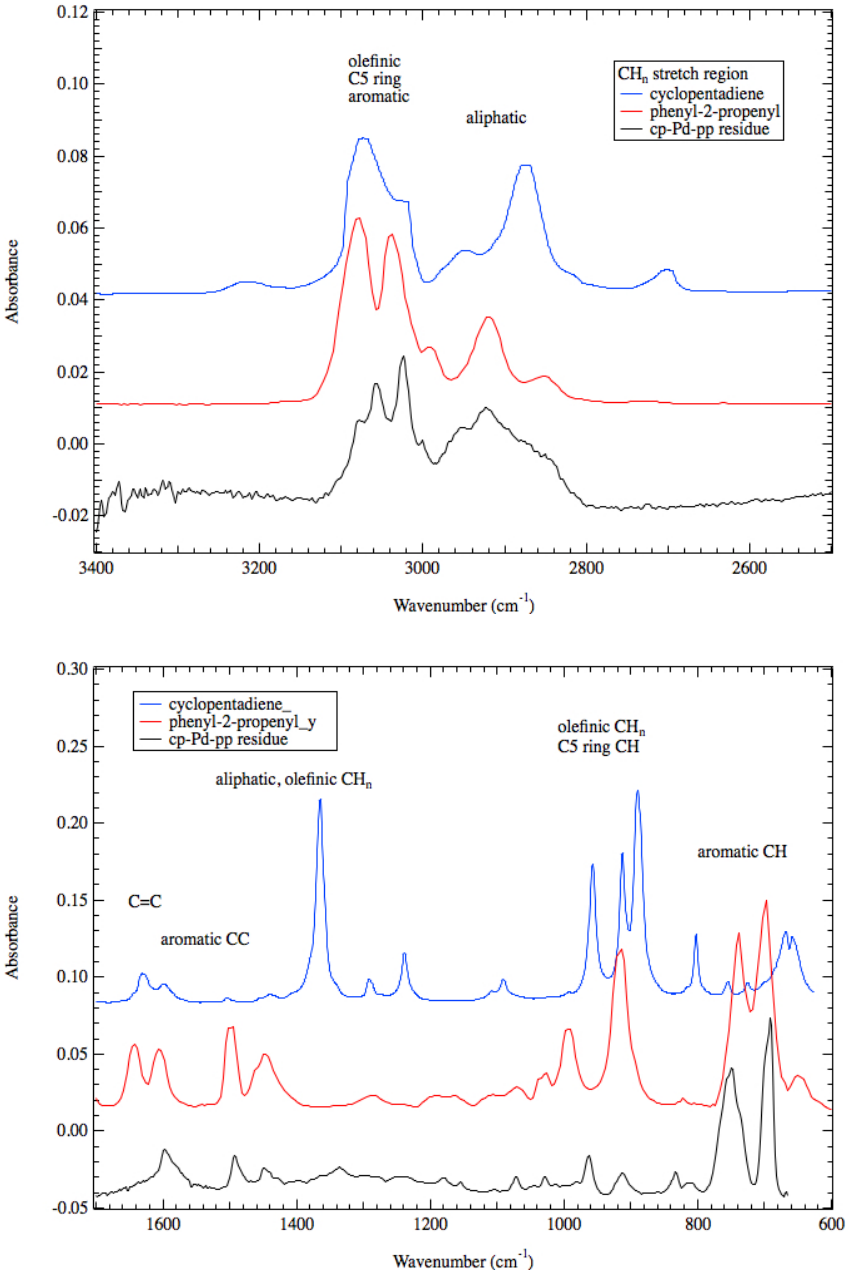

Figure 4-12: IR absorption spectra for the cp-Pd-pp residue created by thermal decomposition during a deposition run.

In principle is should be straightforward to determine the composition and structure of vapor deposited cp-Pd-pp using techniques such as ion beam backscattering and IR absorption spectroscopy. However in the course of these experiments it was found

that the sticking coefficient of cp-Pd-pp is highly dependent on substrate, and quite low in most cases. This complicated efforts to deposit material onto substrates that are convenient for ion beam or IR methods. It is fortuitous indeed for this Project that the sticking coefficients for silicone and DEB appear to be fairly large! However, Figure 4-13 illustrates that even within the class of silicone materials, significant differences are seen. The Figure shows photographs of cp-Pd-pp films vapor deposited onto four different types of silicone: M9763, M9777, Sylgard 184, and DC745. The differences in colors between the samples are striking, suggesting significant variations in the chemistry of the interaction between the substrate and the impinging cp-Pd-pp vapor. This may be caused by differences in the silicone preparation related to catalyst, accelerator, filler, etc. This will be a subject of extensive future study.

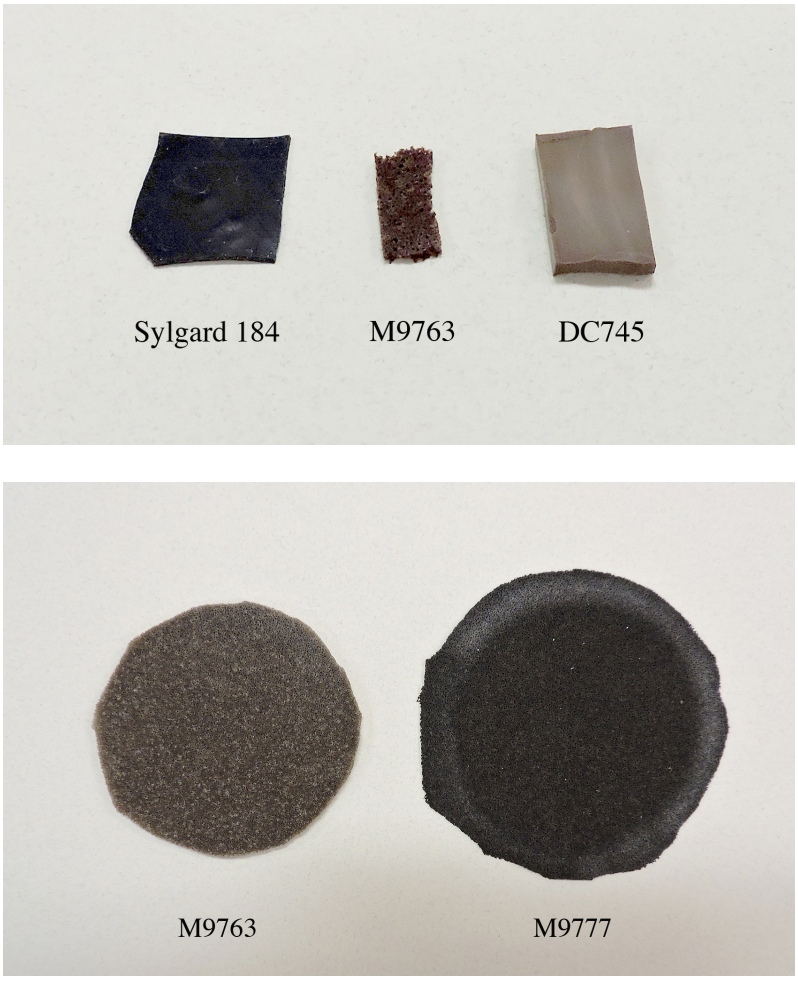

Figure 4-13: Photographs of cp-Pd-pp films vapor deposited onto four different types of silicone: M9763, M9777, Sylgard 184, and DC745.

Ion beam backscattering data for vapor deposited cp-Pd-pp are presented in Figure 4-14, and illustrate how the substrate dependences discussed above complicate attempts to measure film composition. The top plot shows data for material deposited onto Sylgard

184. As seen above in Fig. 4-13 this appears to produce a thick deposit, black in color, that should be easy to characterize. However, inspection of the sample reveals that the deposit has in fact infiltrated throughout the depth of the sample, despite the fact that this substrate is nominally non-porous. This greatly "dilutes" the backscattering signal from the deposited material, complicating analysis. It is possible to determine a ratio of Pd/Si = 0.007 for the top few microns. However, the signal from carbon and oxygen present in the silicone overwhelms that of the deposit, so that Pd/C/O ratios for the deposit can not be determined. The lower plot shows data for material deposited onto a beryllium substrate. Use of this low-Z substrate should easily enable determination of the deposit composition. However the sticking coefficient in this case is very low – the deposit is so thin that only a very small backscattering signal is seen even for Pd. In this case the signal from C and O in the deposit is totally overwhelmed by surface contamination of the beryllium. As a result of these substrates issues, no reliable determination of the deposit composition has yet been made.

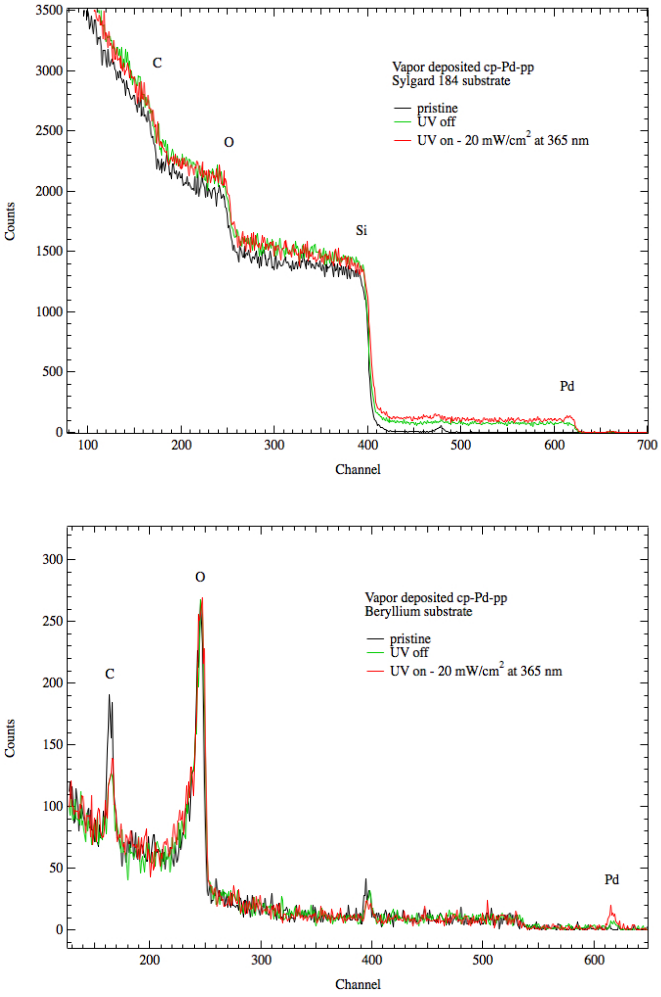

Figure 4-14: Ion beam backscattering data for cp-Pd-pp vapor deposited onto Sylgard 184 (top) and beryllium (bottom). Data are shown for material deposited with and without UV exposure, and also for the bare substrates as reference.

The variability of sticking coefficient also hindered efforts to determine the structure of vapor deposited cp-Pd-pp by IR absorption spectroscopy. The initial approach was to deposit a coating onto an IR transparent substrate, specifically KCl. However no deposition was observed on this material.

A number of polymer substrates were examined as well. These generally have too much background absorption to be useful as IR substrates, but it was hoped that the data might provide some insight into what types of surface chemistry provide for a higher sticking coefficient. The most successful substrates turned out to be the sticky side of Scotch type, which uses an acrylate adhesive, and UV-cured acrylate resin. This suggests an affinity for C=O and/or C-O groups. However this is not a sufficient condition – no deposition was observed on shiny, very smooth, PMMA film. The tape and UV-cured resin both had a relatively rough, matt finish, suggesting that mechanical factors also play a role in the sticking probability of cp-Pd-pp. A similar effect was observed for polyethylene. No deposition was observed on a shiny low-density sample, while slight deposition was seen on a matt high-density sample.

Silicone does provide a relatively high sticking coefficient. However, it exhibits very strong and broad absorption features throughout much of the IR region, making samples of this type impractical for IR analysis. An attempt was made to use Raman spectroscopy for the analysis of silicone coated samples, as the background absorption bands are weaker in this case. Data were taken using a Raman microscope equipped with a 532 nm laser. The results are shown in Figure 4-15 for cp-Pd-pp vapor deposited onto Sylgard 184, both with and without UV exposure. Only two absorption features can be seen for the deposit: a very broad feature with a maximum at 1600 cm^{-1} and extending to about 1150 cm^{-1}, and a very small feature at 1000 cm^{-1}. These features can possibly be attributed to aromatic CC and $=CH_2$, respectively, consistent with the presence of the pp ligand. Recall from the discussion above that the deposit actually infiltrated throughout the depth of the Sylgard substrate. This greatly dilutes the absorption signature of the deposit relative to the substrate, rendering useful analysis impossible.

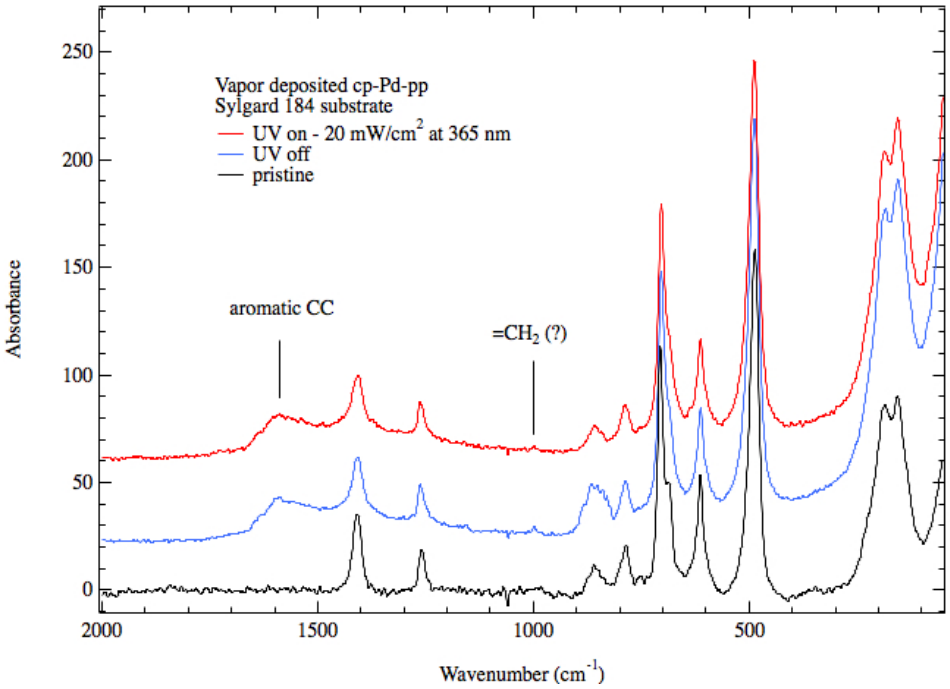

Figure 4-15: Raman spectroscopy data for cp-Pd-pp vapor deposited onto Sylgard 184, both with and without UV exposure. Data for bare Sylgard are also shown as a reference.

Two other experiments were performed using IR spectroscopy in an attempt to determine the structure of vapor deposited cp-Pd-pp. The first of these is a comparison of vapor deposited DEB and vapor co-deposited DEB/cp-Pd-pp. The samples in each case were powdery deposits that covered a portion of a foam substrate configured for forced-flow infiltration. The powder was removed from the substrate and examined by FTIR-ATR. The results are shown in Figure 4-16. Additional absorption features seen in the co-deposited material are found at 3300 cm^{-1} (-OH), 2968 cm^{-1} ($-CH_3$), 1261 cm^{-1} (probably C-O), and possibly a broad feature centered at 1060 cm^{-1} (C-O-C or C-O-H). These data primarily suggest reaction of the cp-Pd-pp deposit with oxygen and/or water vapor, but do not provide useful information on the presence or absence of the cp and pp ligands.

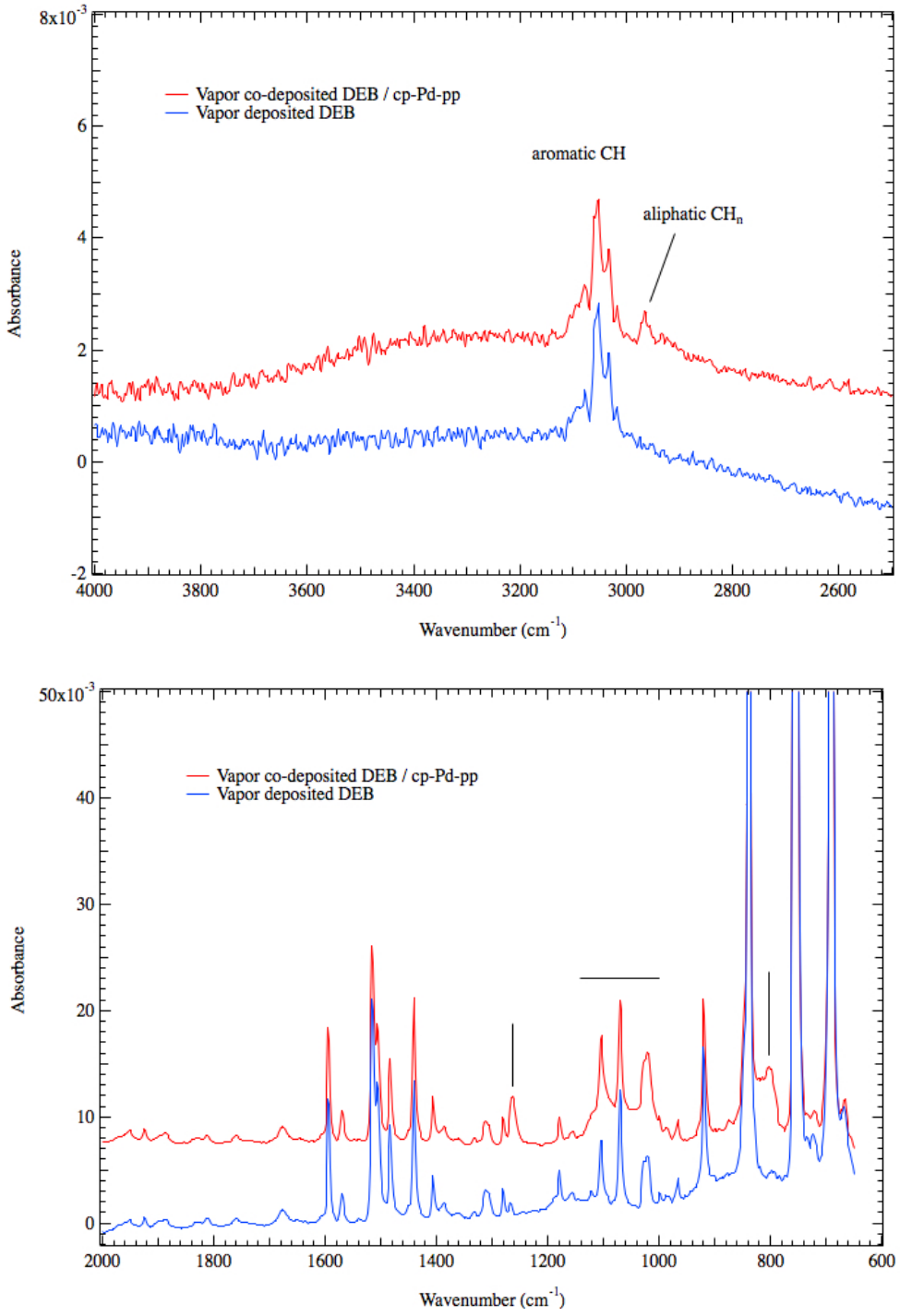

Figure 4-16: IR absorption data for vapor deposited DEB and vapor co-deposited DEB/cp-Pd-pp.

The second test was intended to exploit the relatively high sticking factor of cp-Pd-pp on DEB. For this experiment a thin film of pure DEB was first deposited onto an IR transparent KCl substrate. The DEB source was then turned off and a thick layer of cp-Pd-

pp was deposited onto the DEB surface. IR absorption data for this sample are shown in Figure 4-17, along with reference data of a pure DEB film on KCl, and cp-Pd-pp powder. Comparison of the spectra shows that numerous peaks can potentially be attributed to the cp-Pd-pp film. However the features are generally rather weak, and do not correspond to the patterns present in pristine cp-Pd-pp. In particular, the stronger absorption features seen in pristine cp-Pd-pp are not present for the vapor deposited material. Broadly speaking the observed features are at least consistent with the presence of $-CH_2-$, aromatic rings, C5 rings, C=C, and C=C. The data are therefore consistent with the relatively intact deposition of cp-Pd-pp, but are by no means conclusive.

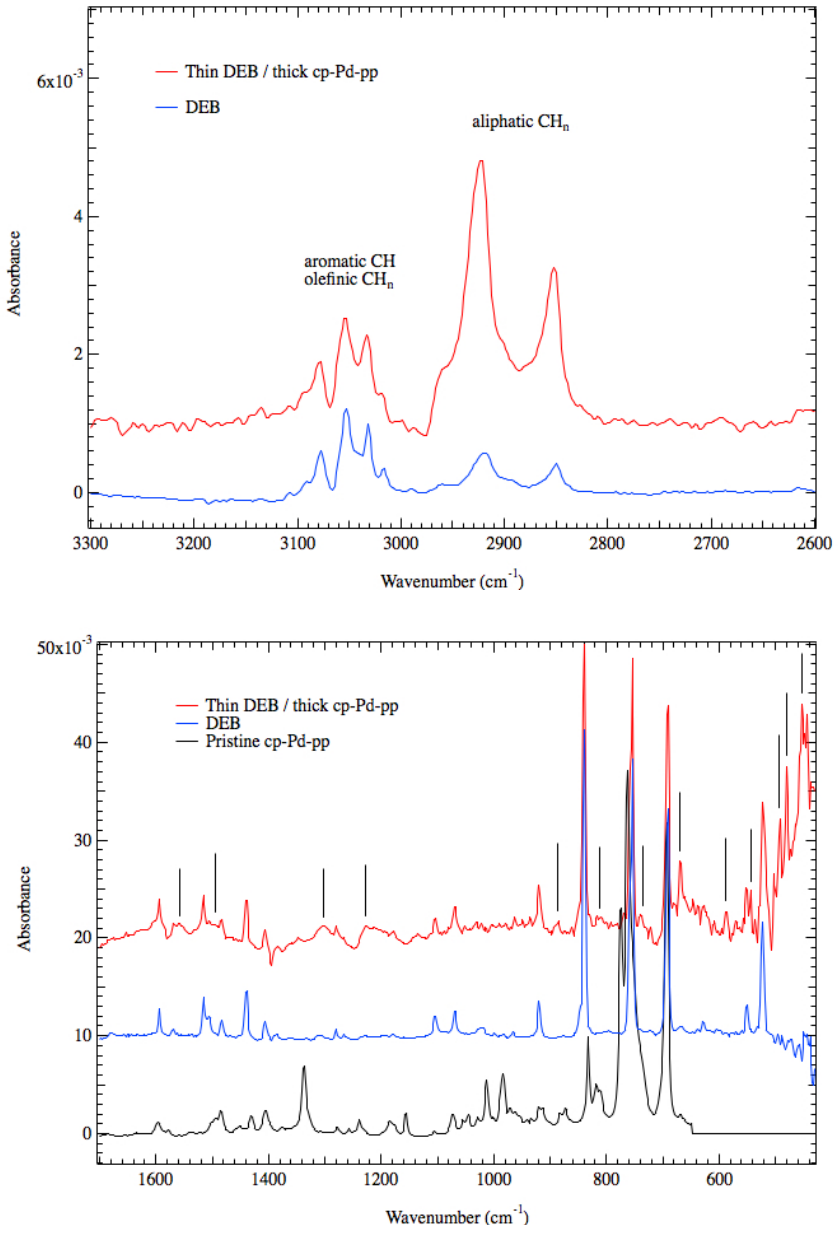

Figure 4-17: IR absorption data for a thick cp-Pd-pp film vapor deposited onto DEB/KCl. Also shown for reference are data for vapor deposited DEB and pristine cp-Pd-pp.

Ultimately the most revealing data related to the structure of vapor deposited cp-Pd-pp come from the hydrogenation tests. These tests demonstrate clearly that the deposit does react with hydrogen to the extent of 3.5-4.0 mole H_2/mole cp-Pd-pp. This indicates that the deposition is close to stoichiometric, even if there is some alteration of the molecular structure. This was confirmed by the proof-of-principle RGA experiments, which clearly showed the presence of volatile C3-C10 species after hydrogenation.

5: Vapor Co-deposition of DEB / cp-Pd-pp

5a: Effects of UV Exposure on Hydrogenation

The experiments performed on the vapor deposition of pure cp-Pd-pp suggest that UV irradiation of the precursor plume during deposition has little effect on the composition or structure of the deposited material. Regardless of UV exposure, it appears likely that the precursor is deposited largely intact, reacts readily with hydrogen (under the conditions studied), and forms volatile species upon hydrogenation.

Subsequently, these experiments were extended in order to investigate the effects of UV exposure on the vapor co-deposition of DEB/cp-Pd-pp. Samples were prepared in the forced flow configuration using 1 mm thick M9777 foam substrates prepared at KCNSC. The deposition conditions were chosen to provide a nominal composition of 9.5 wt% Pd metal. The hydrogen getter performance was quantified as described in Section 2. UV irradiation of the cp-Pd-pp vapor plume was provided by an external UV LED operating at 365 nm and 15-25 mW/cm^2, as described in Section 4a.

Reaction vs. time data are shown for representative samples in Figure 5-1, normalized to the nominal DEB content. The initial reaction rate is seen to be higher for the sample prepared with UV exposure. The data were examined in more detail in order to assess the significance of this observation. The initial portion of the reaction curves was fit by a double exponential function, and the fit functions were then differentiated to provide the reaction rate as a function of time. The results are shown in Figure 5-2. The initial reaction rate is found to be a factor of 3x higher for the sample prepared with UV exposure. However the enhanced rate is very short lived – within 30 sec the rates for the two samples are nearly equal.

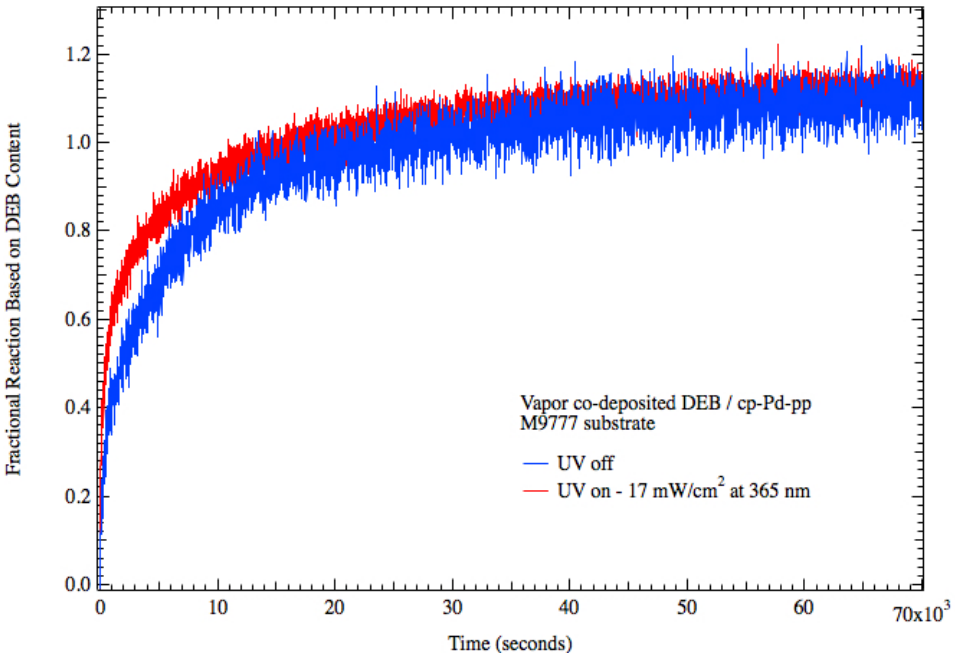

Figure 5-1: Hydrogenation vs. time data for M9777 samples vapor infiltrated with DEB/cp-Pd-pp.

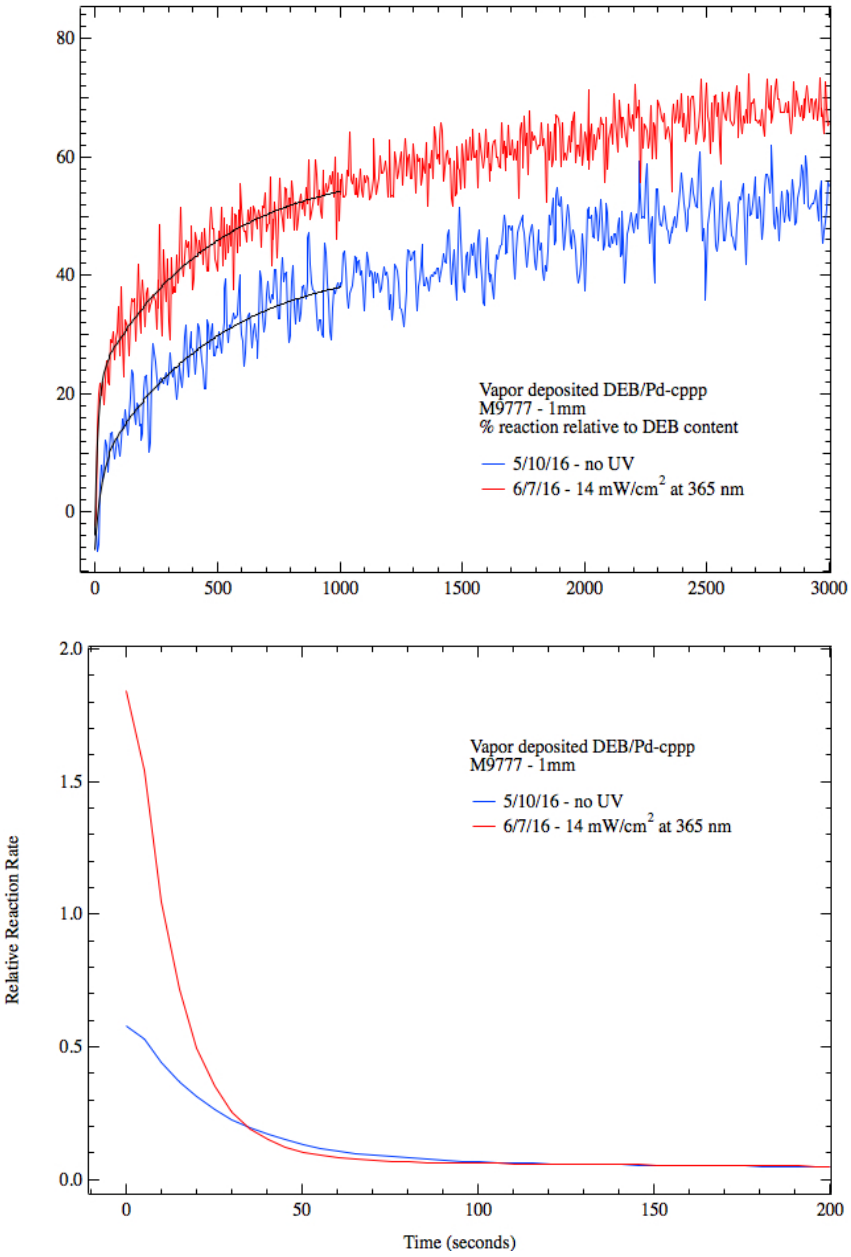

Figure 5-2: Hydrogenation vs. time data for M9777 samples vapor infiltrated with DEB/cp-Pd-pp. The top plot shows the initial portion of the data along with double-exponential fits. The bottom plot shows the fitted data differentiated with respect to time, providing reaction rate.

Despite the apparent difference in the initial reaction rates the total extent of hydrogenation for the two samples, relative to DEB content, is found to be equal within experimental uncertainties. The results are 111% and 112% for the UV off and on samples, respectively. These results imply that the cp-Pd-pp deposit contributes significantly to getter capacity for co-deposited material as well. It is possible to estimate the degree of cp-Pd-pp hydrogenation given an assumption on the degree to which the DEB reacts. If the

final DEB hydrogenation is assumed to be 85%, for example, it is then possible to calculate the amount of excess reacted hydrogen that must have reacted with the cp-Pd-pp. The resulting estimate indicates 51% hydrogenation of the cp-Pd-pp. If the DEB reaction is assumed to proceed to 75%, the estimate for cp-Pd-pp reaction increases to 80%. Thus a plausible estimate for the degree of cp-Pd-pp hydrogenation lies in the range of 50-80%. Note that these results should be considered as lower limits. As was observed for pure cp-Pd-pp samples, the composite samples were found to lose mass during hydrogenation. This implies the formation of volatile species that partially mask the measured pressure drop, so that the calculated extent of reaction is artificially low. The observed mass loss is about 9% with respect to the nominal cp-Pd-pp content. This is less than the typical value for pure cp-Pd-pp (15%) consistent with a slightly lower extent of reaction.

In summary, the hydrogenation behavior of vapor deposited cp-Pd-pp appears to be quite similar for the pure and co-deposited forms of the material. In each case the compound appears to be deposited substantially intact and reacts readily with hydrogen to form (in part) volatile species. Furthermore, the influence of UV exposure during deposition appears to have a minimal influence on the getter behavior of the co-deposited material.

The morphologies of samples prepared with and without UV exposure are shown in the SEM images in Figure 5-3. Also shown are C and Pd elemental maps prepared using SEM/EDS. The secondary electron images suggest that both samples have a continuous, though very rough and irregular, film structure. However, the sample prepared with UV exposure appears to have a slightly higher concentration of surface grains. These grains clearly show up in the C map for this sample. In contrast the Pd map is relatively featureless, showing no correlation with the C map, suggesting a fairly uniform distribution of Pd within the film structure. This implies that the surface grains must be composed primarily of DEB. Note that the UV beam passes only through the cp-Pd-pp vapor plume, not the DEB. If the (slight) change in morphology is caused by the UV exposure, it must therefore be an indirect effect. For example, slight changes in the molecular structure of the cp-Pd-pp deposit may in turn cause changes in the nucleation and growth behavior of the DEB deposit. The net effect of a significant concentration of DEB surface grains on getter behavior is uncertain. On one hand this would cause an overall increased segregation between the catalyst and getter, which would tend to reduce the rate of hydrogenation. On the other hand it would increase the DEB surface area, which could increase the hydrogenation rate. The experimental data in Fig. 5-1 may suggest the latter, though it is not yet proven that the observed difference in UV on vs. off data is truly significant compared with the variations that would be seen for a population of samples prepared under the same conditions. Also, it will be seen below that the effect of UV exposure is in any event much smaller than the effect of substrate properties.

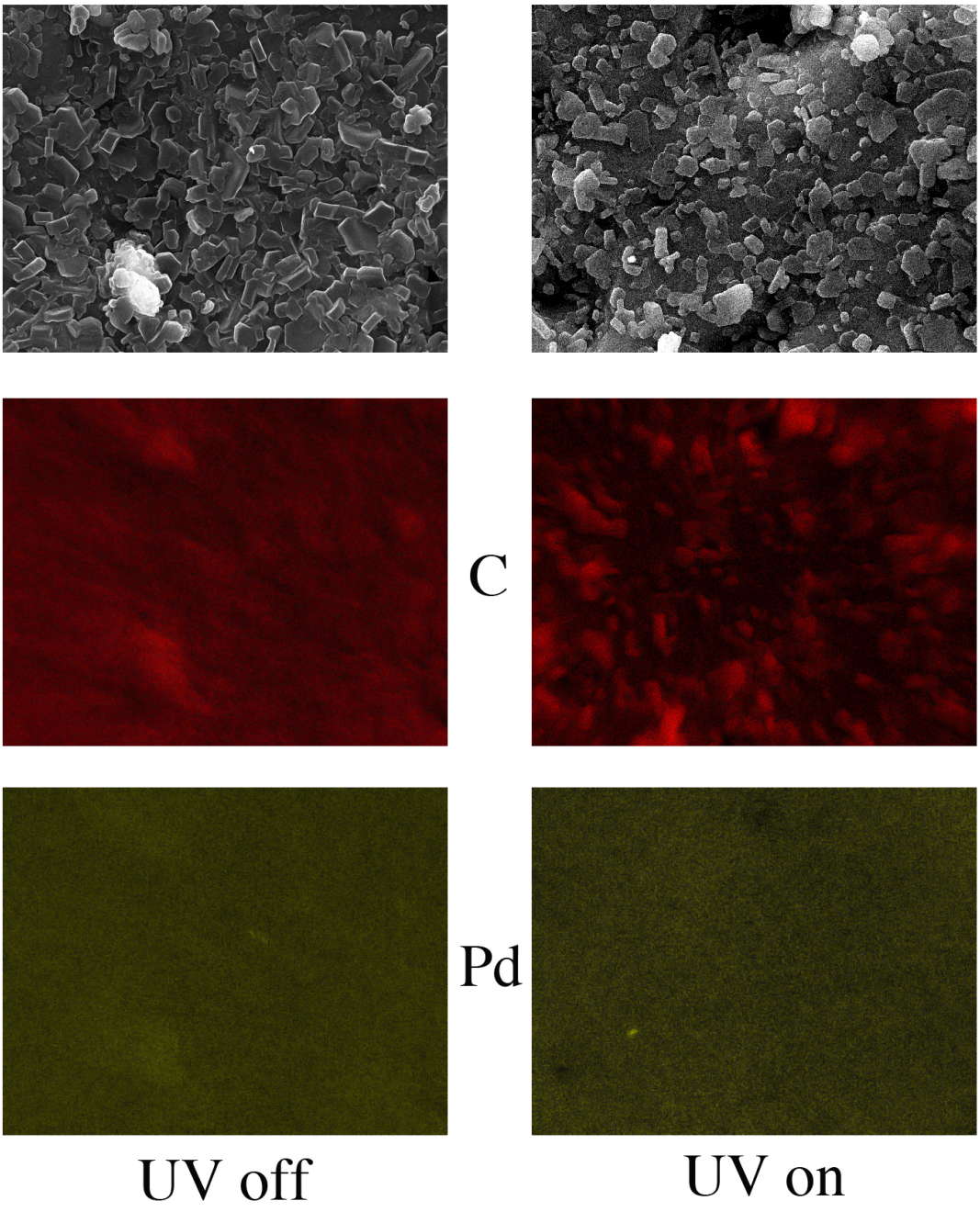

Figure 5-3: SEM and EDS data for vapor co-deposited samples prepared with and without UV exposure during deposition.

In Section 4 it was noted that the physical appearance (at least) of pure vapor deposited cp-Pd-pp films is strongly dependent on substrate, even for different types of silicone. The same is found to be true for co-deposited DEB/cp-Pd-pp samples. Figure 5-4 shows getter composite of the same nominal composition vapor infiltrated into two different types of silicone foam prepared at KCNSC: M9763 and M9777. The material

deposited onto M9777 is found to be much darker – almost black – suggesting a change in the structure/chemistry of the cp-Pd-pp component.

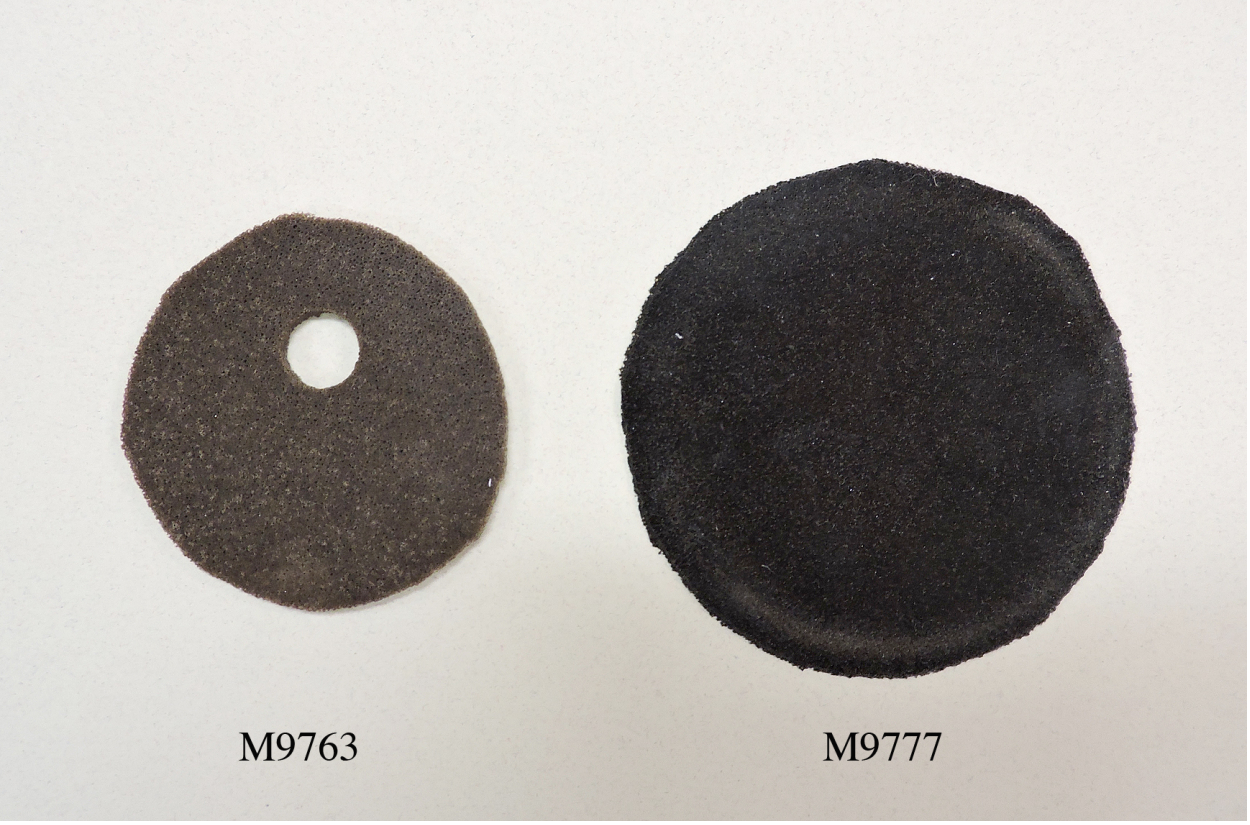

Figure 5-4: Photographs of M9763 and M9777 silicone foams vapor infiltrated with the DEB cp-Pd-pp getter composite.

Significant differences have also been observed in the getter performance of samples prepared using different substrates. Reaction vs. time data for M9777 and another KCNSC foam, M9747, are shown in Figure 5-5. The data are normalized with respect to DEB content in the top plot, and DEB + cp-Pd-pp content in the bottom plot. The data for M9777 are the same as shown in Fig.5-1, and have already been discussed. The early stage reaction kinetics for the M9747 samples are found to be significantly faster than for M9777, and the total extent of reaction is noticeably greater. The extrapolated total reaction for M9777, based on the DEB + cp-Pd-pp content, was found to be 76-82%. The corresponding value for M9747 is 82-89%.

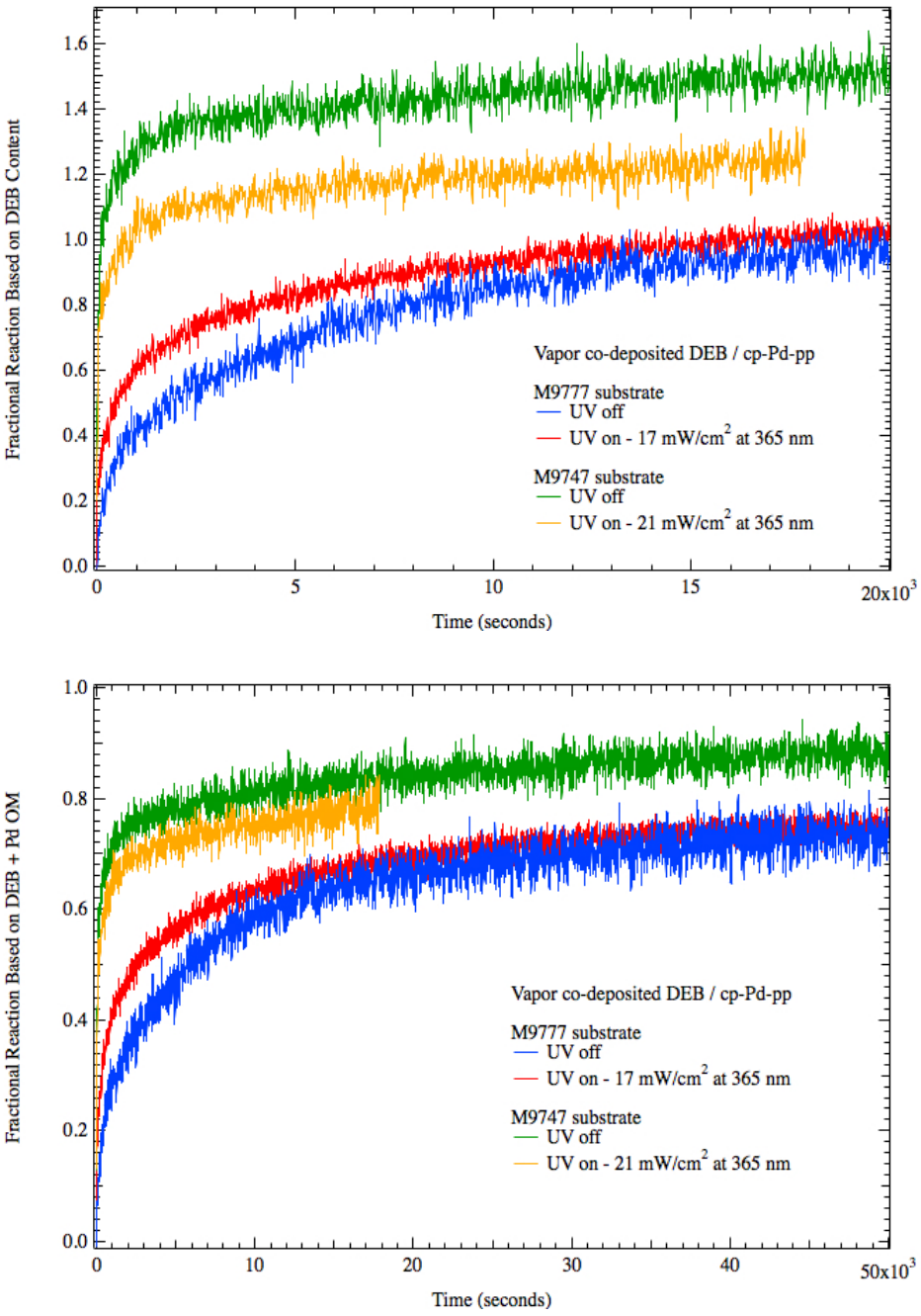

Figure 5-5: Hydrogenation vs. time data for M9777 and M9747 foams vapor infiltrated with DEB/cp-Pd-pp. The data in the top plot are normalized to DEB content, and for the bottom plot normalized to DEB + cp-Pd-pp content.

The cause for the difference in hydrogenation between the M9777 and M9747 samples is not known. One possibility relates to the foam porosity. Transport of cp-Pd-pp vapor is much more efficient than DEB vapor through the thickness of an open-cell foam substrate, resulting in a significant composition gradient as a function of depth. However M9747 has a nominal porosity of 47%, vs. 77% for M9777. It may be that the reduced

porosity inhibits cp-Pd-pp transport significantly, increasing the Pd/DEB ratio near the surface. This in turn might cause more efficient hydrogenation of the DEB. However it should be noted that the mass loss of the M9747 samples during hydrogenation was ~27% with respect to the cp-Pd-pp content. This is considerably higher than observed for the M9777 samples, suggesting that the greater reaction of the M9747 samples may in large part be due to enhanced hydrogenation of the cp and pp ligands from the Pd organometallic. This may imply in turn that differences in substrate (and hence cp-Pd-pp deposit) chemistry are the primary cause. Several types of silicone foam are currently under consideration for applications in the near future. Clearly additional work will be required in order to better understand the effects of substrate properties on getter performance, as this may be a significant factor in the eventual material selection.

Finally, note that for M9747 substrates the sample prepared *without* UV exposure exhibits a higher degree of reaction than the sample prepared with UV exposure. This is opposite to the trend observed for the M9777 samples. However in each case the apparent effect of UV exposure is small, and indeed considerably smaller than the effect of changing substrate. It will therefore also be necessary for future studies to obtain better statistics on run-to-run variations, in order to determine if the observed UV effects are statistically significant.

In conclusion, it is interesting to compare the hydrogenation behavior of DEB/catalyst composites prepared by vapor vs. solution infiltration. Figure 5-6 shows reaction vs. time data for material vapor infiltrated onto M9747 and M9777 substrates, without UV exposure. Data are also shown for a solution-infiltrated sample prepared using toluene. In each case the results are normalized to the total DEB + Pd organometallic content. The initial reaction kinetics for the solution sample are intermediate between those for the two vapor deposited samples. The extrapolated extent of reaction however is found to be significantly lower for the solution sample, at 67%. However, the data discussed previously indicate that the Pd compound used for solution infiltration does not contribute to getter capacity, at least for samples prepared using toluene. In fact hydrogenation proceeds to 81% when normalized to DEB content only, comparable to the estimated DEB consumption for vapor infiltrated samples. This represents a tradeoff between the two infiltration processes as they currently stand. Solution infiltrated samples will have a slightly lower hydrogen capacity for a giving mass of getter. However, these samples can be loaded to higher levels of getter content, and the resulting getter composite appears unlikely to produce a high concentration of volatile products during hydrogenation.

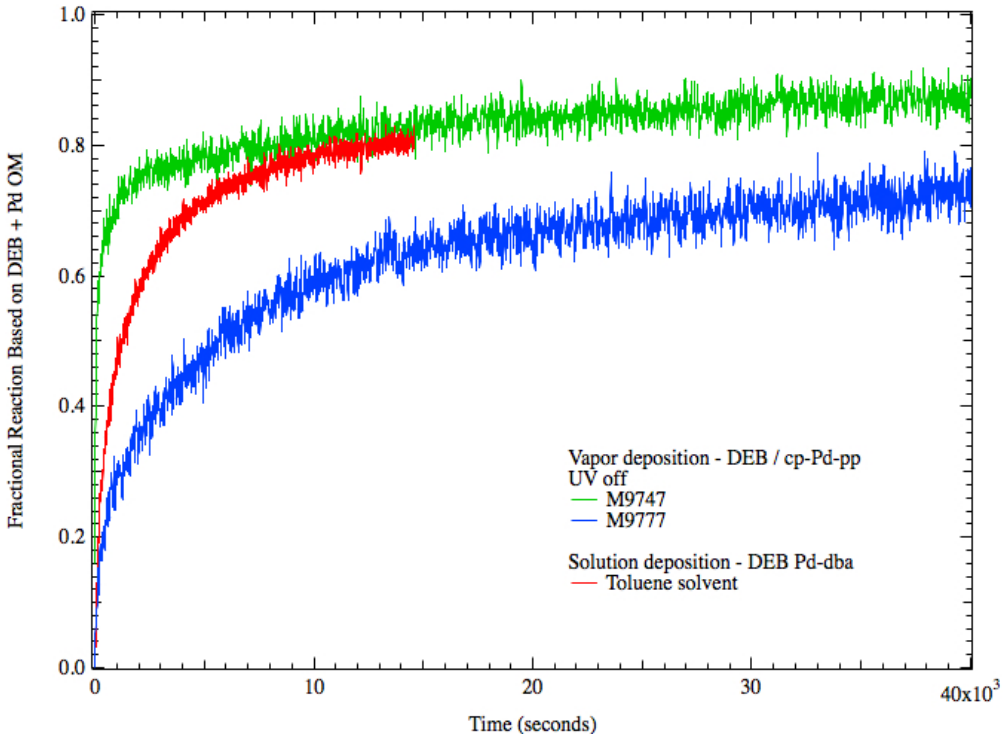

Figure 5-6: Hydrogenation vs. time data for getter composite material vapor infiltrated onto M9747 and M9777 substrates, without UV exposure. Data are also shown for a solution-infiltrated sample prepared using toluene.

6: Conclusions and Future Work

6a: Solution Deposition

A number of solvents were evaluated for the solution infiltration of silicone foams. Solvents such as ethanol and cyclohexane were found to provide limited solubility for DEB, leading to a particle suspension rather than a true solution. This leads to significant segregation of the getter and catalyst upon recrystallization, and therefore a degradation in getter performance.

In contrast, toluene was found to provide good solubility for both DEB and cp-Pd-pp. A true solution is formed, which leads to improved getter/catalyst mixing upon recrystallization. Benefits can be seen in both hydrogen reaction rate and total extent of reaction. Because toluene causes significant swelling of silicone, there is a potential concern that the mechanical properties of the foam may be degraded. Initial load/displacement tests indicate an 11% decrease in the stiffness of M9763 foam caused by toluene exposure. The decrease is deemed acceptable at this point, so that toluene appears to be the preferred solvent for future work.

Experiments demonstrated that the organometallic catalyst Pd-dba acts as a getter in pure form, although with a very slow reaction rate. However conflicting data were obtained on the state and hydrogenation of the dba ligand for material recrystallized from toluene, depending on whether the recrystallization occurred under homogeneous or

heterogeneous conditions. Data on the later for infiltrated foams suggests that dba does participate in hydrogenation. However there are no data to suggest that volatile species are formed as reaction products.

Solution infiltration has been validated as a viable technique and potentially simpler alternative to vapor infiltration. Foams can be loaded with getter composite to as high as 10 wt%. The resulting deposit is uniform, is robust with good adhesion, and provides 80-90% reaction. Continued development of this process will include the following:

- Role of dba ligand: For the use of toluene as solvent, conflicting data were obtained on the behavior of material recrystallized under homogeneous vs. heterogeneous conditions. This conflict will be resolved with further study. If it is confirmed that dba does contribute to hydrogenation for infiltrated foams, then it will also be necessary to confirm whether or not hydrogenation leads to the formation of volatile species that may be detrimental to long-term stability.
- Mechanical properties: Initial experiments indicated that toluene exposure causes minimal degradation of load/displacement behavior for un-infiltrated foams. These experiments will be extended to include the effects of getter infiltration and hydrogenation, as well as the use of other types of silicone substrates. Finally, other relevant mechanical tests will be performed.
- Manufacturability: Pending appropriate funding, solution infiltration studies related to manufacturability will be performed. Specific issues include solution shelf life, solution reuse, scale-up for multiple/larger substrates, and design of a closed system to capture and recycle evaporated toluene.

6b: Vapor Deposition

Efforts to directly measure the composition and structure of vapor-deposited cp-Pd-pp were severely hindered by a sticking coefficient that is strongly substrate dependent, and quite low in most cases. It is rather fortuitous that adequate deposition does occur on DEB and silicone surfaces. However, even within the family of silicone materials, variations in deposit chemistry are observed. The limited data obtained are consistent with the presence of both cp and pp ligands in the vapor deposited material.

Quantitative hydrogenation data for vapor-deposited cp-Pd-pp show that the material does readily react with hydrogen. Mass *loss* during hydrogenation implies the formation of volatile species, and proof-of-principle RGA and IR gas cell analysis of hydrogenated samples confirm this. Overall, the data are consistent with hydrogenation to 95-100% capacity. This strongly suggests that cp-Pd-pp is deposited largely intact, or at least stoichiometrically.

Higher-power UV LEDs were installed to evaluate the effect of UV exposure of the cp-Pd-pp vapor plume during deposition. No significant changes were observed. This confirms previous data taken with lower-power mercury lamps, and offers the potential to greatly simplify the deposition process.

The hydrogenation behavior of cp-Pd-pp vapor co-deposited with DEB appears to be quite similar to that of the pure material in every respect. For example, variations were observed in the chemistry of the co-deposited material for different types of silicone substrates. These are manifested by the color of the deposit, but also by changes in the hydrogenation behavior. For the substrates studied the extent of reaction, normalized to the total DEB/cp-Pd-pp content, was found to vary in the range of ~79-86%. The average

degree of hydrogenation for the cp-Pd-pp component is estimated to be 50-80%, depending on the assumed DEB consumption.

Continued development of the vapor deposition method will include:

- RGA and IR gas cell measurements: The initial data obtained using these techniques were taken under non-ideal conditions, in order to evaluate the potential of these methods. The results were nonetheless useful, and more suitable test systems will be assembled for further work. The mass/IR spectra of cp-Pd-pp vapor will be measured, in order to obtain additional data related to the structure of the resulting deposit. As-deposited material will be analyzed in order to determine if it contains species that are volatile under ambient conditions. Finally, the volatile species present in hydrogenated material will be further evaluated to determine if they pose a potential long-term problem.
- Substrate effects: The cause of variations in deposit chemistry for different types of silicone substrates is unknown – it may be related to catalyst, accelerator, filler, etc. Several types of silicone foam are currently under consideration for applications in the near future. Additional work will therefore be performed in order to better understand the effects of substrate properties on getter performance, as this may be a significant factor in the eventual material selection.
- Manufacturability: Pending appropriate funding, vapor infiltration studies related to manufacturability will be performed. Specific issues include modification of precursor sources, especially for DEB, to improve the efficiency of usage; modification of source temperature vs. time profiles in order to minimize precursor (especially cp-Pd-pp) decomposition; and design of chamber and gas inlet designs to enable uniform infiltration into larger/multiple substrates.

Acknowledgments

The authors would like to thank the W88 Program Office for funding this work.

References

[1] D.W. Carroll, K.V. Salazar, M. Trkula, and C.W. Sandoval, US Patent 6,426,314 (July 30, 2002).
[2] K.V. Salazar, D.W. Carroll, M. Trkula, and C.W. Sandoval, App. Surf. Sci., 214 (2003) 20.
[3] J.N. Lee, C. Park, and G.M. Whitesides, Anal. Chem. **75** (2003) 6544.
[4] L.G.R. Treloar, *The Physics of Rubber Elasticity*, Oxford Classic Texts, 2005.
[5] T. Ukai, H. Kawazura, Y. Ishii, J.J. Bonnet, and J.A. Ibers, J. Organomet. Chem., 65 (1974) 252.
[6] S.S. Zalesskiy and V.P. Ananikov, Organometallics, 31 (2012) 2301.
[7] www.thorlabs.com.
[8] www.mdcvacuum.com
[9] webbook.nist.gov.